

Research Article

# Advancement of Graphite-Clay Composite Electrodes via Different Compositions to Improve the Synergetic Matrix Effect Towards General Electroanalytical and Energy Storage Applications

Pannilage M. H. Madhushanka<sup>1</sup>, Kohobhange S. P. Karunadasa<sup>2</sup>, D. J. D. S. Gamage<sup>3</sup>

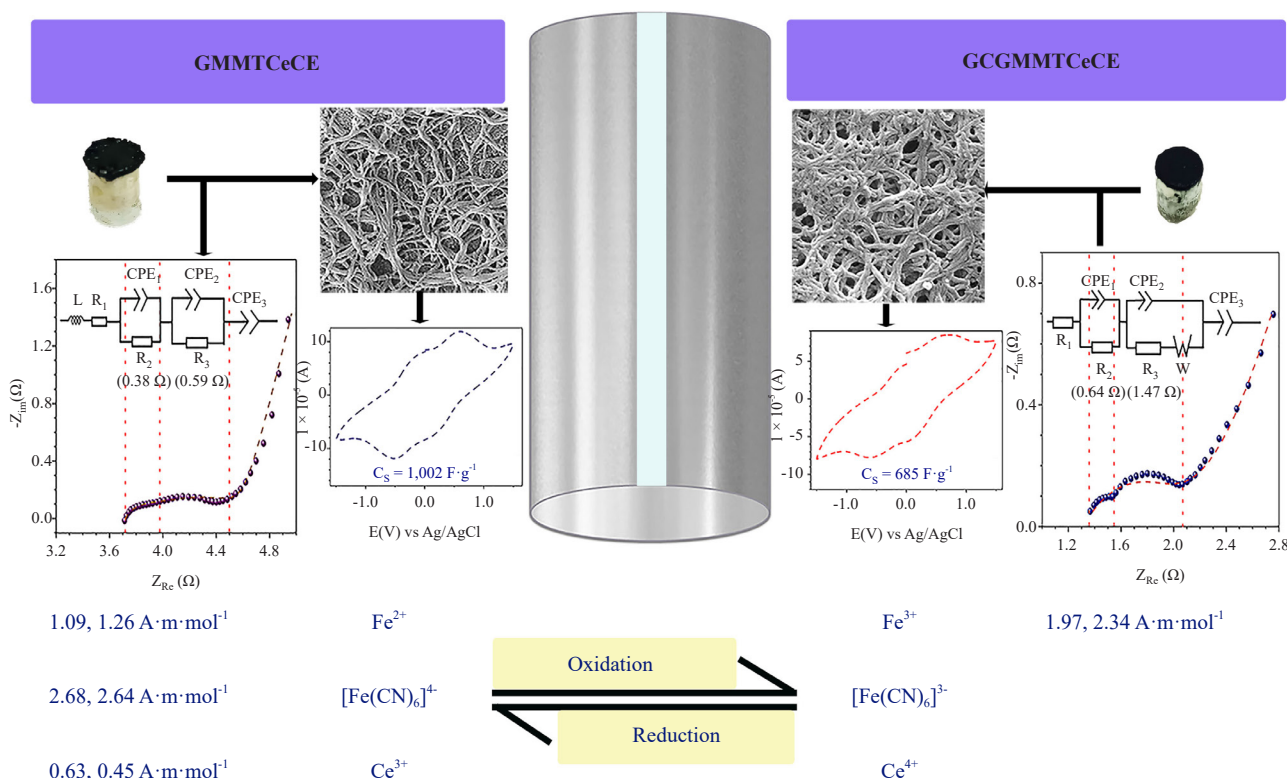
<sup>1</sup>Postgraduate Institute of Science, University of Peradeniya, Peradeniya (20400), Sri Lanka

<sup>2</sup>Materials Technology Section, Industrial Technology Institute, No. 363, BaudhalokA·mawatha, Colombo 7 (00700), Sri Lanka

<sup>3</sup>Department of Environmental and Industrial Sciences, Faculty of Science, University of Peradeniya, Peradeniya (20400), Sri Lanka  
 E-mail: sujith@iti.lk

Received: 16 August 2024; Revised: 27 September 2024; Accepted: 29 September 2024

## Graphical Abstract



**Abstract:** Modern electrode technology trends for enhancing multifunctional electrodes, prioritizing energy storage and electroanalytical prospects. This study anticipates fabricating electrodes by incorporating cement and colloidal graphite, to improve the performance via synergetic interactions of the composite matrix. Graphite-montmorillonite-cement ternary composite electrode (GMMTCeCE) and graphite-colloidal graphite-montmorillonite-cement quaternary composite electrode (GCGMMTCeCE) are fabricated, as two types of electrodes. GMMTCeCE reflects the lowest peak-to-peak separation in  $\text{Ce}^{3+}/\text{Ce}^{4+}$  (0.098 V), greater sensitivity towards  $[\text{Fe}(\text{CN})_6]^{4-}$  ( $2.68 \text{ A} \cdot \text{m} \cdot \text{mol}^{-1}$ ) and  $[\text{Fe}(\text{CN})_6]^{3-}$  ( $2.64 \text{ A} \cdot \text{m} \cdot \text{mol}^{-1}$ ), showing comparatively better performance in analyte detection than GCGMMTCeCE. Multilayered polyaniline (PANI) nanofibers network, which is unique in GMMTCeCE electropolymerization, accounts for very low serial ( $0.38 \Omega$ ) and charge transfer ( $0.59 \Omega$ ) resistances, while densely packed nanofibers of PANI in GCGMMTCeCE is responsible for the lowest ohmic resistance ( $1.31 \Omega$ ). Supercapacitor device fabricated by PANI-GMMTCeCE, achieved higher capacitance ( $1,002 \text{ F} \cdot \text{g}^{-1}$  at  $5 \text{ mV} \cdot \text{s}^{-1}$ ) and showed greater cyclic stability, in contrast to relatively lower specific capacitance ( $685 \text{ F} \cdot \text{g}^{-1}$  at  $5 \text{ mV} \cdot \text{s}^{-1}$ ) attained by PANI-GCGMMTCeCE, demonstrates the superiority of the supercapacitor of GMMTCeCE over GCGMMTCeCE for energy-storage purposes. Therefore, GMMTCeCE outperformed GCGMMTCeCE in electroanalysis and energy storage, confirming better synergetic interactions of the ternary composite matrix over the quaternary one. Besides, further improvements in graphite-clay composite matrix properties facilitate the advancement of electrochemical sensors and supercapacitor devices.

**Keywords:** ternary composite electrode, quaternary composite electrode, analyte detection, electropolymerization, supercapacitor

## 1. Introduction

The graphite-clay composite electrode, which has received escalating attention recently due to better performance over commercial electrodes, is still under development to improve the electrode performance towards different applications, including energy storage and general electroanalytical techniques [1, 2]. This binder free electrode is well tolerated at different temperatures and can be integrated with general electroanalytical applications due to chemical inertness. The electrode matrix improvement received unprecedented attention since the graphite-clay composite electrode is found to be a potential candidate for energy storage applications [3]. However, the matrix improvement can be done either by changing the composition or engineering aspects that are typically involved in the fabrication process. The matrix reengineering has been initiated by advancing binary composite electrodes to ternary electrode, which consists of an additional phase in addition to graphite and clay [4, 5]. However, the matrix effect on performance is studied limiting to one electrode type but a systematic comparison of different electrode compositions has not yet been initiated. Therefore, the present study is dedicated to fabricating new ternary and quaternary graphite-clay composite electrodes and determining the electrode performance under different aspects as a comparison.

Graphite itself reflects several advantages, including chemical inertness, hazard-free cleaning, easy processing, better stability in aqueous solutions, and selectivity enhancement through various modifications, which are vital for electrode application [6, 7]. However, graphite in association with inorganic binders/ionic liquids has many drawbacks, including high contact resistance, a narrow potential range, low viscosity, and low current density [6, 8]. Such failures can be easily eliminated by combining graphite with various mineral phases rather than using binders/ionic liquids. The mineral phase should have certain properties, including low cost, easy integration, and processing to produce composite materials with improved electrical and mechanical stability. Clay is a better choice recently used as a mineral phase, which aligns with all the selection criteria to be eligible as a binder and matrix entrapment agent in composite electrodes [1, 2]. The major raw materials that are mainly used in composite electrodes are graphite and clay, which together account for the electrode conductivity and mechanical strength. Graphite is available in highly pure form and is an inexpensive raw material for electrode fabrication in combination with clay, which is also inexpensive and freely available.

As each study is confined to one type of graphite composite electrode, the present study presents a comparison study of two novel graphite composite electrodes, including ternary and quaternary types. The graphite composite electrodes are frequently subjected to significant compositional changes, with an emphasis on energy storage and general electroanalytical applications, resulting in more fascinating performance. All graphite composite electrodes

fabricated thus far have a narrow potential range and high sensitivity in analyte detection, while electropolymerization produces polyaniline nanofiber networks (PANI) [1, 2, 4, 5, 9]. The latter is responsible for having very high specific capacitance, which is measured using a device fabricated with polyaniline coated graphite composite electrodes [3, 4, 9]. The supercapacitor device fabricated using two identical quaternary electrodes consists of PANI coated graphite-colloidal graphite-kaolinite-cement electrode (GCGKCeCE) accounts for the highest specific capacitance, which is  $1,029 \text{ F}\cdot\text{g}^{-1}$ , revealing the composite electrode's true commercial value [9].

This study demonstrates the fabrication of new ternary and quaternary graphite clay composite electrodes, including graphite-MMT-cement composite electrode (GMMTCeCE) and graphite-colloidal graphite-MMT-cement composite electrode (GCGMMTCeCE). Fabrication is achieved by modifying the graphite-MMT core by incorporating additional mineral phases, including colloidal graphite and cement to improve the performance. The colloidal graphite was recently incorporated in graphite-clay composite electrodes and found to be a better matrix enrichment agent that strengthens the effective electrical contact between the graphite layers [4, 9]. In contrast, a recent study found that cement is a better agent for enriching the mechanical framework, resulting in a strong graphite-clay composite electrode [5]. Therefore, the colloidal graphite and cement are better matrix enrichment agents that can easily integrate with graphite-clay composite electrodes even following a similar fabrication process, which was often used in the author's previous work. As usual, the electrode performance is determined in terms of analyte detection and electropolymerization, but with new strategies, which improves the quality of final data presentation. These two new composites are also employed in supercapacitor device fabrication, which helps to determine the modified electrode potential in energy storage applications. This study aims to correlate the electrodes' performance with composition and determine how effective the new electrodes are in energy storage and electroanalytical applications compared to other electrodes, including commercial and existing graphite composite electrodes.

## 2. Experimental

### 2.1 Materials

The primary raw materials of the composite electrodes, including natural graphite (> 99.9%, average particle size  $3.1 \mu\text{m}$ ) and colloidal graphite (99.9%, average particle size  $1.0 \mu\text{m}$ , Aquadag G303E) that were acquired from Bogala Graphite Lanka PLC, Sri Lanka, and Agar Scientific Ltd, UK, respectively. The secondary raw materials, including MMT clay (> 99%, average particle size  $4.5 \mu\text{m}$ ) and cement (> 98%, average particle size  $1.5 \mu\text{m}$ ) were supplied from Sigma-Aldrich Ltd, USA, and the Department of Geology, University of Peradeniya, Sri Lanka, respectively. Inorganic analytes, including Ammonium ferrous sulfate hexahydrate [ $> 99.5\%$ , AFSH,  $(\text{NH}_4)_2\text{Fe}(\text{SO}_4)_2\cdot 6\text{H}_2\text{O}$ ], Potassium hexacyanoferrate(II) trihydrate [99%, PHCFT,  $\text{K}_4\text{Fe}(\text{CN})_6\cdot 3\text{H}_2\text{O}$ ], and Cerium(IV) sulfate tetrahydrate [ $> 98\%$ , CST,  $\text{Ce}(\text{SO}_4)_2\cdot 4\text{H}_2\text{O}$ ] were purchased from Sigma-Aldrich Ltd, USA, Merck chemicals, USA, and BDH Chemicals, UK, respectively. KCl (> 99.5%) utilized as a background electrolyte was procured by Sigma-Aldrich Ltd, USA. The chemical reagents, including HCl (> 37%) and  $\text{H}_2\text{SO}_4$  (98%) were obtained from Sigma-Aldrich Ltd, USA. Aniline (> 99.5%) employed as an organic analyte was supplied from Honeywell Riedel-de Haen, Germany, was doubly distilled before use and stored in a refrigerator.

### 2.2 Fabrication of GMMTCeCE and GCGMMTCeCE

The electrodes were fabricated by pursuing the standard methods, which were introduced by previously fabricated graphite-clay composite electrodes and changing the process parameters slightly to optimize the fabrication process [1, 2, 5]. Composite of GMMTCeCE was prepared by mixing graphite, MMT, and cement in 16:3:1 ratio by weight, whereas the graphite, colloidal graphite, MMT, and cement were mixed by 8:8:3:1 ratio by weight to obtain GCGMMTCeCE composite. Both composites were mixed separately using deionized water, followed by stirring for 2 h at 360 rpm by an overhead stirrer (IKA Labortechnik, Germany). Then, they were subjected to dry completely at  $120 \text{ }^\circ\text{C}$  for 48 h in a laboratory oven (Menmert, Germany). GMMTCeCE and GCGMMTCeCE were fabricated by pressing 3 g of dried composites in a specially designed stainless-steel mold using a manual hydraulic press under the ram force of  $2.2 \times 10^4 \text{ N}$ , followed by firing in a tube furnace (ELITE TMH 12/75/750) at  $550 \text{ }^\circ\text{C}$  for 1 h.

### 2.3 Characterization of GMMTCeCE and GCGMMTCeCE

The resistance of each electrode was measured by linear sweep voltammetry (LSV) operated from 0 V to 0.5 V at 20 mV·s<sup>-1</sup> using Biologic SP 150 Potentiostat/Galvanostat (France). The resistivity of each electrode was calculated based on equation 1 [10].

$$\rho = \frac{RA}{l} \quad (1)$$

Where  $\rho$ ,  $R$ ,  $A$ , and  $l$  are the resistivity, resistance, cross-sectional area ( $7.86 \times 10^{-5} \text{ m}^2$ ), and length of the electrode, respectively. The flexural strength of each electrode was determined by modulus of rupture (MOR) analysis using a Testometric universal testing machine (UK), and the values of flexural strength of the electrodes were calculated according to equation 2 [11].

$$\sigma = \frac{FL}{\Pi r^3} \quad (2)$$

Where the flexural strength, the force at the fracture point, the length of the supporting span (2.0 cm), and the radius of each electrode (0.5 cm) are defined by  $\sigma$ ,  $F$ ,  $L$ , and  $r$ , respectively. The morphology of the horizontal cross-section of both electrodes was observed by scanning electron microscopy (SEM, ZEISS EVO LS15, Germany) under a magnification of ( $\times 40,000$ ) at the tube voltage of 20 kV.

### 2.4 Electrochemical performance of GMMTCeCE and GCGMMTCeCE

The capability of electrochemical performance of GMMTCeCE and GCGMMTCeCE as working electrodes was compared in the analyte detection and electropolymerization using Biologic SP 150 Potentiostat/Galvanostat (France). Concerning the analysis, both electrodes (1.0 cm in length) were fabricated and modified by inserting Cu wire ( $> 99\%$  purity,  $\text{Ø}$  1.0 mm) as a power-supply terminal. The side surfaces of the electrodes were uniformly covered with insulating paint (Nippon, Japan) in multiple layers and the electrodes' bottom surfaces were precisely reshaped by reducing the electro-active surface area ( $\text{Ø}$  3.0 mm, cross-sectional area of  $7.07 \times 10^{-6} \text{ m}^2$ ) through the coating of the insulating paint, which was utilized in the analyte detection.

Analyte detection related to the inorganic analytes (AFSH, PHCFT, and CST) was performed using cyclic voltammetry (CV) for both electrodes, and resulting voltammograms were obtained. The detection corresponding to  $\text{Fe}^{2+}/\text{Fe}^{3+}$  for both electrodes was achieved using freshly prepared AFSH ( $50 \text{ mmol}\cdot\text{dm}^{-3}$ ) in acidified (0.1 M HCl) KCl (1 M) as background electrolyte. PHCFT ( $50 \text{ mmol}\cdot\text{dm}^{-3}$ ) in 1 M KCl as background electrolyte was utilized to determine  $\text{Fe}^{2+}/\text{Fe}^{3+}$  detectability for both electrodes and glassy carbon (GCE) and Pt disc (PtE) electrodes. To determine the  $\text{Ce}^{3+}/\text{Ce}^{4+}$  redox probe for both electrodes and commercial electrodes, including GCE and PtE, CST ( $50 \text{ mmol}\cdot\text{dm}^{-3}$ ) was prepared before the analysis using 0.1 M  $\text{H}_2\text{SO}_4$  background electrolyte [12, 13]. The sensitivity of each electrode towards the model analytes was assessed with different analyte concentrations using square wave voltammetry (SWV). The peak currents related to the various concentrations of both analytes were measured for each electrode. The working electrodes' sensitivities were estimated by the gradient in the curve between the current density and the analyte concentration.

GMMTCeCE and GCGMMTCeCE underwent electropolymerization using Aniline ( $50 \text{ mmol}\cdot\text{dm}^{-3}$ ), an organic monomer dissolved in 1 M HCl, which was the background electrolyte. The process involved ten consecutive cycles of CV to successfully produce polyaniline (PANI) coating. SEM analysis of PANI coated on both electrodes was conducted by observing morphological microstructure under a magnification of ( $\times 50,000$ ) at the tube voltage of 20 kV using an SEM instrument (ZEISS EVO LS15, Germany). To characterize the electrochemical structure of PANI, Nyquist plots were obtained for both supercapacitor cells using Electrochemical Impedance Spectroscopy (EIS), executed from 100 kHz to 10 mHz [4].

**Table 1.** CV and SWV parameters utilized in the analyte detection and electro-polymerization processes

Analysis	Analyte	BGE	C (mmol·dm <sup>-3</sup> )	WE	Parameter			
					E (V)	v (mV s <sup>-1</sup> )	N <sub>c</sub>	
Analyte detection	AFSH	1 M KCl in acidified with 0.1 M HCl	50	GMMTCeCE	-0.1 to 1.0	25	3	
				GCGMMTCeCE	-0.1 to 1.0			
				GMMTCeCE	0.3 to 0.9			
				GCGMMTCeCE	0.3 to 0.9			
	PHCFT	1 M KCl	50	GCE	-0.4 to 0.8	25	3	
				PtE	-0.4 to 1.0			
				GMMTCeCE	0.8 to 1.7			
				GCGMMTCeCE	0.8 to 1.7			
	CST	0.1 M H <sub>2</sub> SO <sub>4</sub>	50	GCE	0.5 to 1.8	25	3	
				PtE	0.7 to 1.7			
				GMMTCeCE	0.8 to 1.7			
				GCGMMTCeCE	0.8 to 1.7			
Sensitivity	AFSH	1 M KCl in acidified with 0.1 M HCl	4 × 10 <sup>-3</sup> , 4 × 10 <sup>-2</sup> , 2 × 10 <sup>-1</sup> , 1, 5, 25, 50, 100	GMMTCeCE	-0.1 to 1.0	25	1	
				GCGMMTCeCE	-0.1 to 1.0			
				GMMTCeCE	-0.1 to 0.9			
				GCGMMTCeCE	-0.1 to 0.9			
	PHCFT	1 M KCl	50	4 × 10 <sup>-4</sup> , 4 × 10 <sup>-3</sup> , 4 × 10 <sup>-2</sup> , 2 × 10 <sup>-1</sup> , 1, 5, 25, 50, 100	GCE	-0.3 to 1.0	25	1
					PtE	-0.3 to 1.0		
					GMMTCeCE	0.8 to 1.7		
					GCGMMTCeCE	0.8 to 1.7		
	CST	0.1 M H <sub>2</sub> SO <sub>4</sub>	50	4 × 10 <sup>-3</sup> , 4 × 10 <sup>-2</sup> , 2 × 10 <sup>-1</sup> , 1, 5, 25, 50	GCE	0.5 to 1.8	25	1
					GMMTCeCE	0.8 to 1.7		
					GCGMMTCeCE	0.8 to 1.7		
					GCE	0.5 to 1.8		
Electro-polymerization	Aniline	1 M HCl	50	GMMTCeCE	-0.5 to 1.2	25	10	
				GCGMMTCeCE	-0.5 to 1.2			
Electro-polymerization for Supercapacitor cell	Aniline	1 M HCl	50	GMMTCeCE	-0.5 to 1.2	25	100	
				GCGMMTCeCE	-0.5 to 1.2			

BGE-Background electrolyte, C-Analyte concentration, WE-Working electrode, E-potential range (potential window), v-scan rate, N<sub>c</sub>-Number of scan cycles, M = mol dm<sup>-3</sup>, GCE-Glassy carbon electrode (Ø 3.00 mm, electrode surface area of 7.07 × 10<sup>-6</sup> m<sup>2</sup>, ALS Co. Ltd, Japan), PtE-platinum electrode (Ø 1.60 mm, electrode surface area of 2.01 × 10<sup>-6</sup> m<sup>2</sup>, ALS Co. Ltd, Japan)

All electrochemical parameters employed in CV and SWV techniques were summarized in Table 1. All electrochemical measurements were carried out using a three-electrode system comprising of the reference electrode [Ag/AgCl electrode, ALS Co. Ltd, Japan,  $E = +0.205$  V vs. standard hydrogen electrode], platinum wire as the counter electrode (Pt wire, ALS Co. Ltd, Japan), and working electrode of interest. Prior to the analysis, PtE and GCE were persistently polished using alumina suspension supported of an alumina polishing pad supplied by ALS Co. Ltd (Japan). The analyte solutions were degassed with high purity, oxygen-free-nitrogen gas for 30 min before each of the electrochemical analysis.

## 2.5 Fabrication of energy-storage devices (supercapacitor cells)

The model supercapacitor cells were developed using PANI-coated GMMTCeCE and GCGMMTCeCE to assess the feasibility of energy storage device applications. Each device was constructed by sandwiching two identical segments of PANI-coated electrode (0.5 cm in length) between two equivalent filter papers as the separator, which soaked in 1 M  $H_2SO_4$ . PANI-coated electrode segments were created by electro-polymerization of aniline, to form a thin layer of PANI in 100 cycles of CV on the entire bottom surface of both electrodes ( $\varnothing$  1.0 cm, cross-sectional area  $7.86 \times 10^{-5}$  m<sup>2</sup>). To evaluate the performance of each type of electrode's supercapacitor cell, the solid-state CV was performed at different scan rates (starting from  $5 \text{ mV}\cdot\text{s}^{-1}$  and increasing by  $5 \text{ mV}\cdot\text{s}^{-1}$  intervals up to  $25 \text{ mV}\cdot\text{s}^{-1}$ ). The specific capacitance of each supercapacitor cell was calculated using the integrated area in CV according to equation 3 [3, 4].

$$C_S = \frac{\int_{V_a}^{V_c} I_V dV}{mv(V_c - V_a)} \quad (3)$$

The parameters, including  $C_S$  (specific capacitance in  $F\cdot g^{-1}$ ),  $(V_c - V_a)$  (potential window in V),  $m$  (mass of active material in g), and  $v$  (scan rate in  $\text{mV}\cdot\text{s}^{-1}$ ) were used to calculate the specific capacitance. Integration using Origin software was accurately determined by the term  $I_V dV$ , which represented the area under the CV curve. The charge-discharge performance of each device was determined using the galvanostatic charge-discharge with potential limitation (GCPL) technique, conducted within the potential range (from -1 V to +1 V) at  $1 \times 10^{-3}$  A. The Coulombic efficiency demonstrated cyclic stability in each device was calculated by applying equation 4 [14].

$$\eta = (t_d/t_c) \times 100\% \quad (4)$$

Where  $\eta$ ,  $t_d$ , and  $t_c$  represent Coulombic efficiency, discharge time, and charge time, respectively. Specific capacitance of each supercapacitor cell was determined based on Galvanostatic charge discharge curves using equation 5 [15].

$$C_S = \frac{I \times \Delta t}{\Delta V \times m} \quad (5)$$

Where  $C_S$  is specific capacitance,  $I$  is the discharge current,  $\Delta t$  is the discharge time,  $\Delta V$  is potential window,  $m$  is mass of active material (PANI), respectively. All the voltammograms and Nyquist plots were analyzed by EC lab integrated software with SP 150 Biologic Potentiostat/Galvanostat.

### 3. Results and discussion

#### 3.1 GMMTCeCE and GCGMMTCeCE characterization

Two different composite electrodes, GMMTCeCE and GCGMMTCeCE, were fabricated using graphite and MMT as the major core of the matrix and cement incorporated for both electrodes as an additional phase, while GCGMMTCeCE contains colloidal graphite as another additional phase of the composite matrix. Table 2 summarizes the resistivity and mechanical strength of two electrodes: GMMTCeCE has a lower resistivity than GCGMMTCeCE, but both electrodes fall in the semiconductor region based on their resistivity [16]. By comparing with resistivity of previously fabricated graphite-MMT composite electrodes, the order of resistivity variation is as follows: GMMTCE < GMMTCeCE < GCGMMTCeCE < GCGMMTCE [1, 4]. Additional phases of materials incorporation into the graphite-MMT composite matrix resulted in increasing the resistivity, while cement incorporation has a lower effect on resistivity compared to the addition of colloidal graphite. Thus, the GMMTCeCE ternary composite electrode is more effective, in terms of electrical conductivity than the GCGMMTCeCE quaternary composite electrode.

**Table 2.** Resistivity and mechanical strength results of GMMTCeCE and GCGMMTCeCE

Electrode	Resistivity ( $\Omega \cdot m$ )	Flexural Strength ( $N \cdot m^{-2}$ )
GMMTCeCE	$1.59 \times 10^{-3}$	$6.61 \times 10^5$
GCGMMTCeCE	$3.65 \times 10^{-3}$	$1.48 \times 10^7$

Horizontal cross-sectional morphology of both electrodes is shown in Figure 1, illustrating distinct structures associated with each electrode. These morphological structural variations in electrodes may account for the differences in the electrical and mechanical properties of the two electrodes. The microstructure of GMMTCeCE reveals uniformly arranged graphite sheets without any cracking surface of the electrode, resulting in lower resistivity due to proper electrical contact between graphite sheets. On the other hand, in GCGMMTCeCE, colloidal graphite contributes to forming smaller, clusters like graphite sheets on the electrode surface, leading to inconsistent electrical contacts of graphite sheets, resulting in lower conductivity. The incorporation of additional phases in the graphite-MMT matrix accounts for the decrease in conductivity, which is confirmed by the GMMTCE binary electrode has the lowest resistivity among all graphite-MMT type composite electrodes due to it containing only graphite and MMT without any additional phases [1]. However, the low resistivity of GMMTCeCE indicates that the ternary composite matrix effectively reduces the resistivity, leading to the formation of a better conductive structure of the electrode compared to GCGMMTCeCE.

MOR analysis indicates that GCGMMTCeCE has higher strength than GMMTCeCE (see Table 2). The variation of the strength of graphite-clay composite electrodes follows this order: GCGMMTCeCE > GMMTCE > GCGMMTCE > GMMTCeCE [1, 4]. Despite resistivity, the strength variation in graphite-MMT composite electrodes appears irregular behavior by incorporating additional phases into the composite matrix. GCGMMTCeCE quaternary electrode, which contains two additional phases has the highest strength among them, revealing smaller, cluster-type sheets that appeared in SEM morphology contribute to the increase in the strength of the electrode than lamella-like graphite sheets and uniformly arranged graphite sheets. However, the addition of a low percentage of cement (5%) into the composite electrode is less effective for significant changes in the strength of the electrode. However, these results suggest that cement-incorporated GMMTCeCE is prominent in electrical properties and colloidal graphite and cement-incorporated GCGMMTCeCE is dominant in mechanical properties. Therefore, incorporating cement and colloidal graphite into the graphite-MMT composite enhances the synergistic matrix effect, confirming improvements in electrical and mechanical applications.

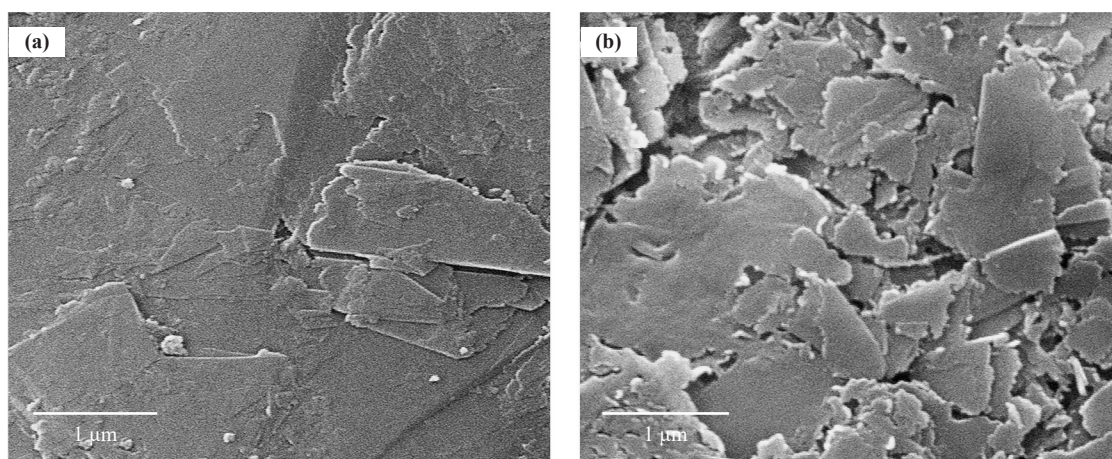


**Figure 1.** Horizontal cross-sectional morphology of electrodes observed from SEM under the magnification ( $\times 40,000$ ); (a) GMMTCeCE (uniformly arranged graphite sheets); (b) GCGMMTCeCE (small, cluster-like graphite sheets)

### 3.2 Analyte detection using GMMTCeCE and GCGMMTCeCE

Two electrodes have demonstrated the ability to detect inorganic analytes by AFSH, PHCFT, and CST model precursors. Detection was possible due to well-resolved oxidation and reduction peaks, as seen in ideal cyclic voltammograms (Table 3 and Figure 2). Square wave voltammograms (as shown in Figure 3) were also utilized to detect  $\text{Fe}^{2+}/\text{Fe}^{3+}$  and  $\text{Ce}^{3+}/\text{Ce}^{4+}$ . Both electrodes exhibit distinguishable cyclic voltammograms for each analyte, indicating their capability to detect various inorganic analytes. These cyclic voltammograms (Figure 2a) are ideal in shape for AFSH analyte similar to GCGMMTCE, showing better performance in analyte detection, compared to previously fabricated graphite-clay composite electrodes and commercial electrodes [1, 2, 4, 9]. Detecting PHCFT analyte, GMMTCeCE has a better CV curve (Figure 2b) in a shape similar to GCE and PtE with lower peak currents (Figure A1.a), but CV in GCGMMTCeCE appears with reduced peaks. When detecting  $\text{Ce}^{3+}/\text{Ce}^{4+}$ , GMMTCeCE and GCGMMTCeCE exhibit ideal CV curves, including oxidation and reduction peaks (Figure 2c). GCE showcases a proper voltammogram in CV, whereas PtE shows a deviated CV profile accompanied by a small reduction peak only within the respective potential window (see Figure A1.b). This can be explained as follows;  $\text{Ce}^{4+}$  is the initial form of analyte, which appears as a yellow-colored solution, later it is reduced to  $\text{Ce}^{3+}$ , resulting in a stable, white-colored precipitate with  $\text{SO}_4^{2-}$  ions in the solution. The concentration of  $\text{Ce}^{4+}$  is greater at the electrode-electrolyte interface than in bulk solution at the early stage in the solutions of carbon-based electrodes, including GMMTCeCE, GCGMMTCeCE, and GCE. While reducing  $\text{Ce}^{4+}$  at the electrode-electrolyte interface,  $\text{Ce}^{3+}$  formation is slowly increasing, limiting the diffusion of  $\text{Ce}^{3+}$  ions into bulk solution, and preventing the formation of precipitates. Conversely, the electrode-electrolyte interface of PtE facilitates for faster reduction reaction, leading to a higher concentration of  $\text{Ce}^{3+}$  ions in the bulk solution, and rapid production of a white-colored precipitate compared to solution systems of carbon-based electrodes. Due to this phenomenon occurring in PtE, it is unable to detect  $\text{Ce}^{3+}$  ions, but  $\text{Ce}^{4+}$  ions can be detected by PtE. Therefore, this demonstrates competency in  $\text{Ce}^{3+}/\text{Ce}^{4+}$  detection by carbon-based electrodes, which is an advantageous feature in both composite electrodes over metal-based electrodes. Although both electrodes show better CV curves, GMMTCeCE displays comparatively better cyclic voltammogram shapes than GCGMMTCeCE for each analyte. Furthermore, SWV curves of both electrodes exhibit ideal shapes (Figure 3), GCGMMTCeCE appears to have a higher current than GMMTCeCE due to a relatively higher background current, which is a disadvantageous feature. Therefore, GMMTCeCE and GCGMMTCeCE account for significant performance in analyte detection for all three analytes, with GMMTCeCE being the most effective electrode. This suggests that uniformly arranged graphite sheets in GMMTCeCE and the ternary composite matrix enhanced the affinity of inorganic ions than small-clustered graphite sheets in GCGMMTCeCE. In that sense, incorporating these additional materials into the composite matrix of the graphite-MMT basic core of electrodes has been shown to reflect significant improvements in analyte detection.

**Table 3.** Numerical results in analyte detection and sensitivity of GMMTCeCE and GCGMMTCeCE determined by CV and SWV

WE		GMMTCeCE			GCGMMTCeCE		
Analyte		AFSH	PHCFT	CST	AFSH	PHCFT	CST
Peak I (Oxidation)	$E_{pa}$ (V)	0.555	0.308	1.305	0.558	0.351	1.322
	$I \times 10^{-3}$ (A)	0.65	0.57	0.16	0.40	1.10	0.16
Peak II (Reduction)	$E_{pc}$ (V)	0.425	0.202	1.207	0.432	0.159	1.210
	$I \times 10^{-3}$ (A)	0.60	0.63	0.17	0.38	1.03	0.52
	$I_{pa}/I_{pc}$	1.08	0.90	0.94	1.05	1.07	0.31
	$\Delta E_p$ (V)	0.130	0.106	0.098	0.126	0.192	0.112
	LOD	1.7 ppm	169 ppb	1.6 ppm	15.7 ppm	169 ppb	16.2 ppm

WE-working electrode,  $I_{pa}$ -anodic peak current,  $E_{pa}$ -anodic peak potential,  $S_A$ -sensitivity of anode,  $I_{pc}$ -cathodic peak current,  $E_{pc}$ -cathodic peak potential,  $S_C$ -sensitivity of cathode,  $\Delta E_p$ -peak-to-peak separation ( $\Delta E_p = E_{pa} - E_{pc}$ ), LOD-limit of detection

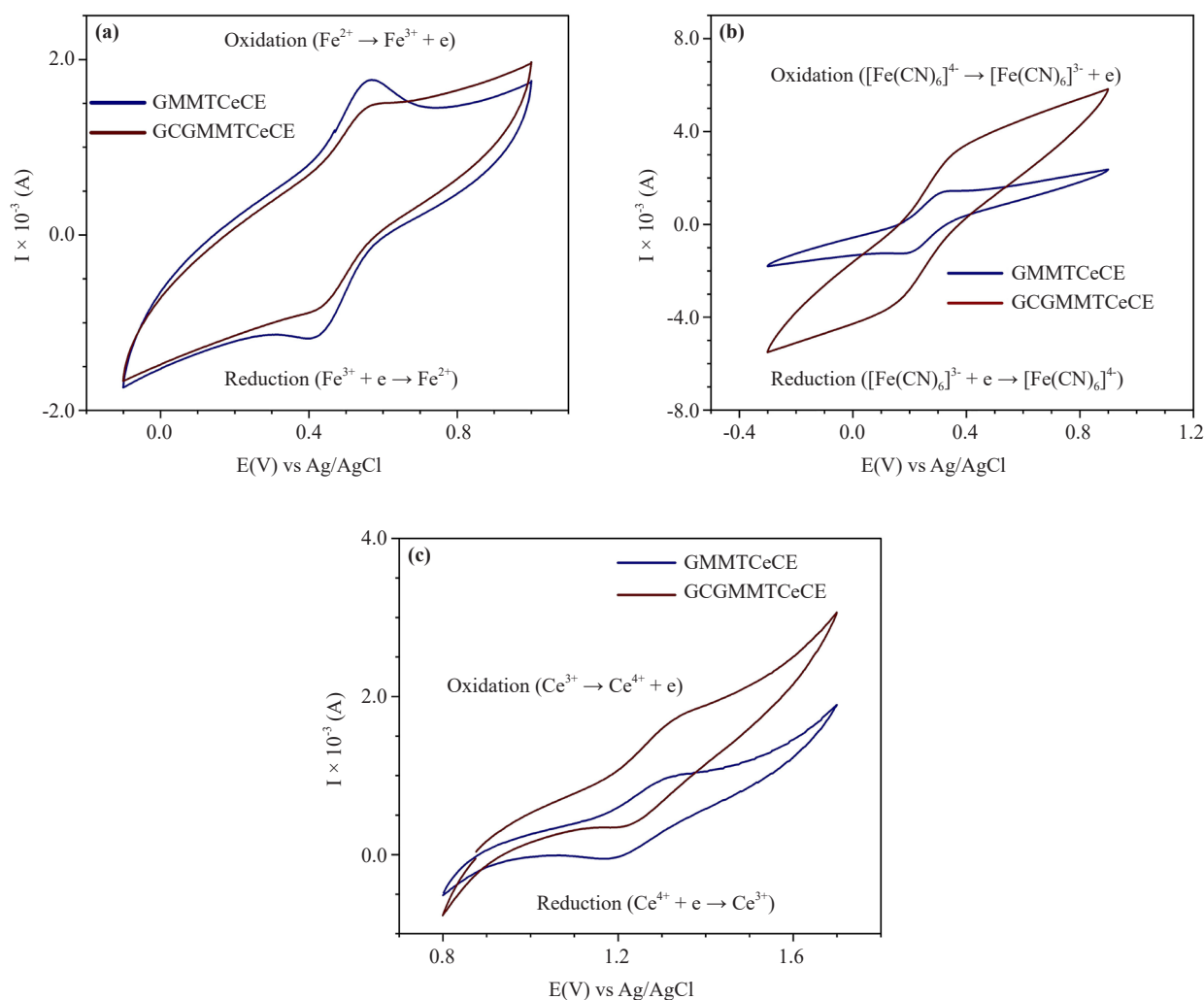


**Figure 2.** Cyclic voltammograms related to the analyte detection with GMMTCeCE and GCGMMTCeCE by different analytes; (a) AFSS; (b) PHCFT; (c) CST

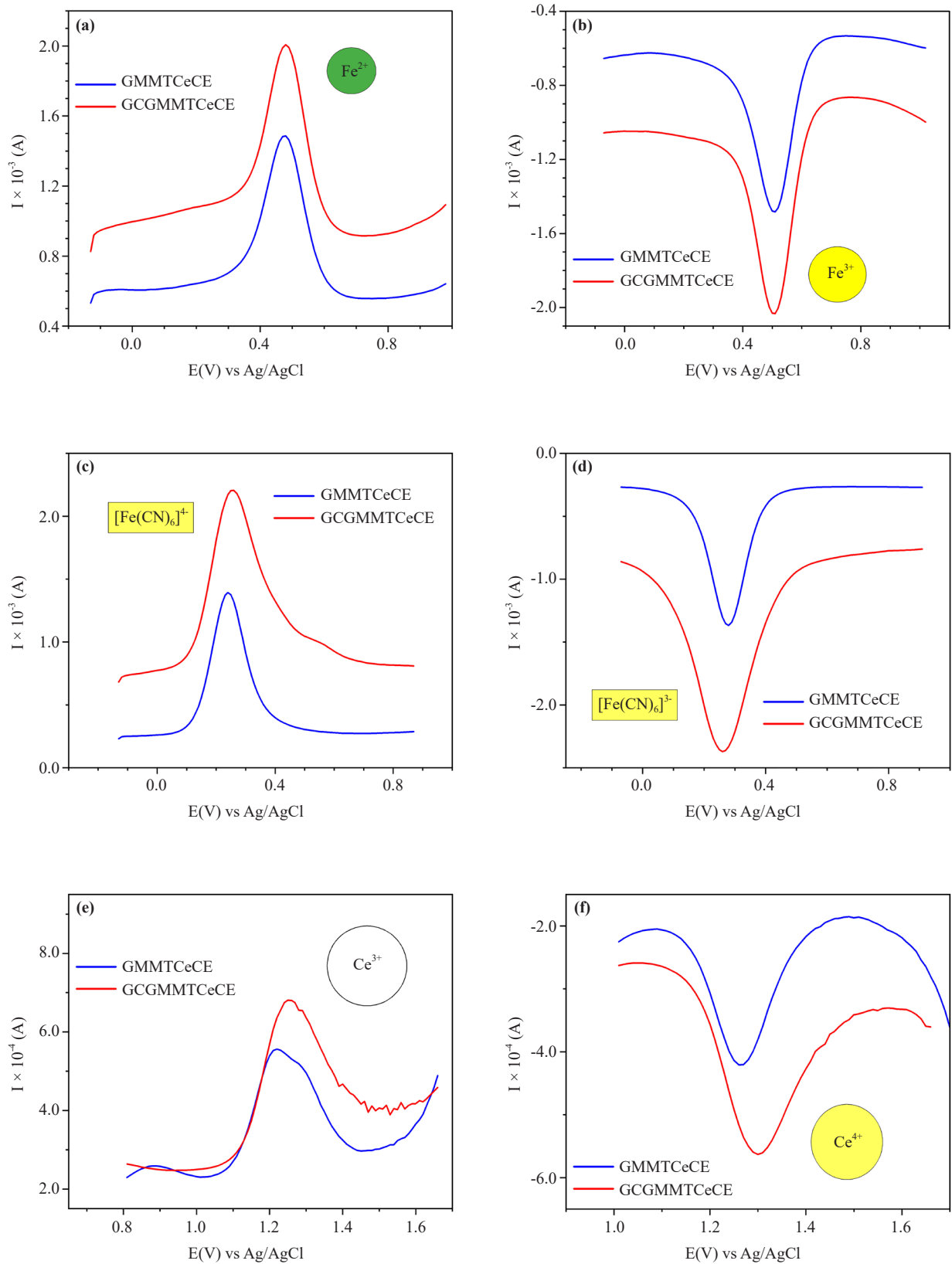


**Figure 3.** Square Wave Voltammograms related to the analyte detection using GMMTCeCE and GCGMMTCeCE with different analytes; (a)  $Fe^{2+}$  detection by AFSH; (b)  $Fe^{3+}$  detection by AFSH; (c)  $[Fe(CN)_6]^{4-}$  detection by PHCFT; (d)  $[Fe(CN)_6]^{3-}$  detection by PHCFT; (e)  $Ce^{3+}$  detection by CST; (f)  $Ce^{4+}$  detection by CST

Peak-to-peak separation ( $\Delta E_p$ ) is the measure of electron transfer kinetics in an analytical system and is used to evaluate the performance of electrodes in analyte detection [2]. Narrow  $\Delta E_p$  indicates a fast electron transfer rate between the analyte and electrode interface, while wide  $\Delta E_p$  suggests to slower heterogeneous electron transfer rate [2]. Both composite electrodes have lower values of  $\Delta E_p$  concerning each analyte (Table 3). For the AFSH analyte, GCGMMTCeCE demonstrates the lowest  $\Delta E_p$  comparatively to all the graphite-clay composite electrodes fabricated up to these, but it is approximately similar to  $\Delta E_p$ (GMMTCeCE), the previously fabricated electrodes, including  $\Delta E_p$ (GCGMMTCE): 0.128 V and  $\Delta E_p$ (GCGKCeCE): 0.138 V [4, 9]. These  $\Delta E_p$  values of both electrodes are significantly lower than values for commercial electrodes, including  $\Delta E_p$ (PtE) and  $\Delta E_p$ (GCE) for AFSH, which indicates that both electrodes are better alternatives in analyte detection than commercial electrodes [4]. To detect  $[\text{Fe}(\text{CN})_6]^{4-}/[\text{Fe}(\text{CN})_6]^{3-}$  by PHCFT analyte, GMMTCeCE depicts the lowest  $\Delta E_p$  than GCGMMTCeCE and GKCeCE (0.122 V), which was fabricated by authors previously [5]. Additionally, for PHCFT,  $\Delta E_p$ (GMMTCeCE) is very close to  $\Delta E_p$ (GCE) (0.104 V) and higher than  $\Delta E_p$ (PtE) (0.070 V), suggesting that GMMTCeCE can perform similarly to graphite-based commercial electrodes (like GCE) than metal electrode (PtE). For CST, both electrodes exhibit lower  $\Delta E_p$ , while  $\Delta E_p$ (GMMTCeCE) is lower than  $\Delta E_p$ (GCGMMTCeCE). GCE has higher  $\Delta E_p$  (0.199 V) compared to GMMTCeCE and GCGMMTCeCE for CST analyte. Lower  $\Delta E_p$  values imply a low energy barrier that supports heterogeneous electron transfer with higher rates [17, 18]. Furthermore, it is advantageous in detecting analytes within the solvent window and preventing solvent electrolysis in the system [2]. It is beneficial for detecting a wide range of analytes within safer limits. Therefore, lower  $\Delta E_p$  values obtained for each analyte in both electrodes, are remarkable achievements with improved electroanalytical performance than previously fabricated graphite-clay composite electrodes and commercial electrodes. GMMTCeCE appears as a better performer than GCGMMTCeCE, considering analyte detection, revealing its better composite matrix and electrode surface capability, to achieve this high performance.

The electrode sensitivity, a significant parameter of performance in the electrode, can be expressed in a linear curve, obtained from current density as a function of analyte concentration. The efficiency of the electrode can be demonstrated by its sensitivity, and the magnitude of sensitivity reflects the nature of interactions between the electrode and analyte [1, 2]. A greater sensitivity can be obtained if the electrode can produce a measurable peak current even at low concentrations. SWV technique is employed to determine the sensitivity of each electrode corresponding to each ion because it can measure the faradic current with a significant reduction of capacitive current and greater sensitivity within a short analysis time [19]. GMMTCeCE and GCGMMTCeCE account for different sensitivities for each analyte ion, which characterize varying behavior of analyte and electrode (see Table 4 and Figure 4).

**Table 4.** Sensitivities of different analytes by electrodes, including GMMTCeCE, GCGMMTCeCE, PtE, and GCE

Type of ions	Sensitivity of Electrode/A·m·mol <sup>-1</sup>			
	GMMTCeCE	GCGMMTCeCE	PtE	GCE
Fe <sup>2+</sup>	1.09	1.96	0.53*	0.16*
Fe <sup>3+</sup>	1.26	2.34	0.55*	0.12*
$[\text{Fe}(\text{CN})_6]^{4-}$	2.68	$J = 44.28 + 4.11 C - 1.64 \times 10^{-2} C^2$	1.44	0.90
$[\text{Fe}(\text{CN})_6]^{3-}$	2.64	$J = 55.65 + 4.43 C - 2.01 \times 10^{-2} C^2$	1.36	0.86
Ce <sup>3+</sup>	0.63	$J = 5.94 + 1.19 C - 1.24 \times 10^{-2} C^2$	-	$J = 44.28 + 4.11 C - 1.64 \times 10^{-2} C^2$
Ce <sup>4+</sup>	0.45	$J = 7.35 + 1.16 C - 1.49 \times 10^{-2} C^2$	-	$6.54 \times 10^{-2}$

*J*-Current density corresponding to each analyte ion, *C*-Concentration of respective analyte solution, \*Sensitivities-Source from [9]

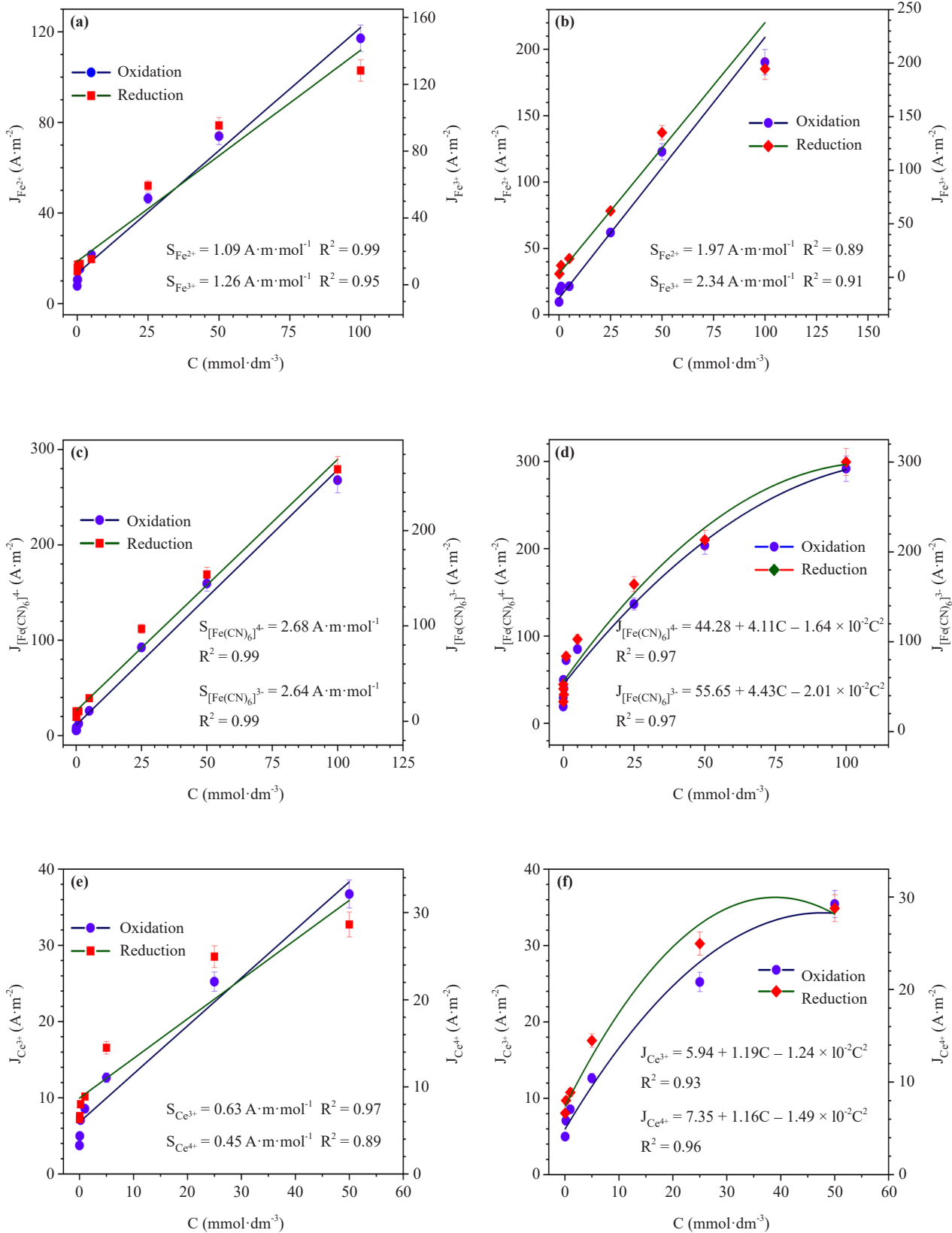


**Figure 4.** Electrodes' sensitivities towards different analyte ions; (a)  $Fe^{2+}/Fe^{3+}$  sensitivities of GMMTCeCe by AFSH; (b)  $Fe^{2+}/Fe^{3+}$  sensitivities of GCGMMTCeCe by AFSH; (c)  $[Fe(CN)_6]^{4+}/[Fe(CN)_6]^{3-}$  sensitivities of GMMTCeCe by PHCFT; (d)  $[Fe(CN)_6]^{4+}/[Fe(CN)_6]^{3-}$  sensitivities of GCGMMTCeCe by PHCFT; (e)  $Ce^{3+}/Ce^{4+}$  of GMMTCeCe by CST; (f)  $Ce^{3+}/Ce^{4+}$  of GCGMMTCeCe by CST [ $J$ ,  $C$ , and  $S$  denote the current density ( $A \cdot m^{-2}$ ), analyte concentration ( $mmol \cdot dm^{-3}$ ), and sensitivity of each analyte species ( $A \cdot m \cdot mol^{-1}$ ), respectively.]

When considering AFSH, which includes free ionic forms of  $\text{Fe}^{2+}$  and  $\text{Fe}^{3+}$ , GCGMMTCeCE shows greater sensitivities towards both ions ( $\text{Fe}^{2+}$  and  $\text{Fe}^{3+}$ ) compared to GMMTCeCE (Table 4 and Figure 4a and 4b). Both electrodes exhibit significantly higher sensitivities, indicating both electrodes can create strong interactions with analyte ions. Variation of sensitivities for AFSH by graphite-clay composite electrodes follows this order: GCGMMTCeCE > GKCE > GMMTCeCE > GCGKCeCE > GCGMMTCE [2, 4, 9]. Additionally, these composite electrodes' sensitivities for  $\text{Fe}^{2+}$  and  $\text{Fe}^{3+}$  ions are much higher than those of commercial electrodes, including GCE and PtE [9]. Therefore, GCGMMTCeCE and GMMTCeCE show that both ternary and quaternary composite electrodes can form stronger interactions between analyte ions and electrodes than commercial electrodes, leading to greater sensitivities.

PHCFT is another type of inorganic analyte, consisting of Fe in coordination complex with six  $\text{CN}^-$  atoms, which can be used to evaluate the detection of  $\text{Fe}^{2+}/\text{Fe}^{3+}$  redox probe similar to AFSH. GMMTCeCE demonstrates greater sensitivity through a linear curve, whereas GCGMMTCeCE exhibits polynomial behavior in detecting  $\text{Fe}^{2+}$  and  $\text{Fe}^{3+}$  ions (refer to Table 4, Figure 4c, and 4d). Therefore, GCGMMTCeCE sensitivities related to  $[\text{Fe}(\text{CN})_6]^{4-}/[\text{Fe}(\text{CN})_6]^{3-}$  can be calculated using the equations provided in Table 4 and Figure 4d. Also, GMMTCeCE shows closely similar sensitivities in magnitudes, indicating that this ternary electrode can detect both  $[\text{Fe}(\text{CN})_6]^{4-}/[\text{Fe}(\text{CN})_6]^{3-}$  with greater accuracy. Furthermore, GMMTCeCE sensitivities to  $[\text{Fe}(\text{CN})_6]^{4-}/[\text{Fe}(\text{CN})_6]^{3-}$  are much greater than PtE and GCE (Figure B1.a and B1.b) similar to AFSH, indicating GMMTCeCE facilitates the generation of powerful interactions between analyte ions with electrode surfaces, as opposed to weaker interactions formations of commercial electrodes. Although AFSH and PHCFT were utilized to determine the detection of the same redox couple ( $\text{Fe}^{2+}/\text{Fe}^{3+}$ ), GCGMMTCeCE performs differently in sensitivity compared to the identical linear behavior of GMMTCeCE. This phenomenon is associated with the non-identical diffusion coefficients of these analytes, it can be expressed in the following Randles-Sevcik equation [17].

$$i_p = 0.446nFAC_0 \left( \frac{nFvD_0}{RT} \right)^{1/2} \quad (6)$$

Where  $i_p$ ,  $n$ ,  $F$ ,  $A$ ,  $C_0$ ,  $v$ ,  $D_0$ ,  $R$ ,  $T$  are defined as peak current, number of electrons transferred in the redox reaction, Faraday constant, electrode surface area, the bulk concentration of the analyte, scan rate, the diffusion coefficient of the analyte, universal gas constant and the absolute temperature, respectively. When determining the sensitivities using AFSH and PHCFT, all the variables are identical for both analytes except the analytes' diffusion coefficients ( $D_0$ ). In AFSH,  $\text{Fe}^{2+}$  is in the free ionic form, while  $\text{Fe}^{2+}$  is in the center of the coordination complex bound with six  $\text{CN}^-$  ligands in PHCFT. Because the chemical nature of  $\text{Fe}^{2+}$  is different from each other, resulted in different  $D_0$  for each analyte. Therefore,  $\text{Fe}^{2+}/\text{Fe}^{3+}$  ions are accompanied at different rates to electrode-electrolyte interface from bulk solution, leading to the generation of non-identical peak currents in similar concentrations' solutions of both analytes.

By CST, the redox behavior of  $\text{Ce}^{3+}$  and  $\text{Ce}^{4+}$  ions are used to assess the detection capability of both electrodes, GMMTCeCE and GCGMMTCeCE. The former exhibits a linear variation curve, while the latter accounts for a polynomial variation curve (Figure 4e and 4f). Due to the different composite matrices of electrodes, the interactions between electrodes and  $\text{Ce}^{3+}/\text{Ce}^{4+}$  redox couple are non-identical, leading to varying sensitivities in both electrodes. GCE cannot produce measurable peak currents in lower concentrations, resulting in inaccurate sensitivity calculation (Figure B1.c). However, the sensitivity of  $\text{Ce}^{3+}$  is calculated using the equation mentioned in Table 4 and Figure B1.c, and  $\text{Ce}^{4+}$  sensitivity is much lower than GMMTCeCE. On the other hand, PtE fails to properly detect cerium ions due to the rapid precipitate formation in the analyte solution as described above, therefore sensitivities cannot be determined for  $\text{Ce}^{3+}/\text{Ce}^{4+}$ . As cerium is comparatively larger and different from iron, GMMTCeCE can detect cerium redox couple more accurately and efficiently than GCGMMTCeCE and commercial electrodes. When comparing the sensitivities of GMMTCeCE and GCGMMTCeCE, GMMTCeCE exhibits significantly higher sensitivities for  $\text{Fe}^{2+}/\text{Fe}^{3+}$  and  $\text{Ce}^{3+}/\text{Ce}^{4+}$  due to the ternary composite matrix, which enhances the properties of the composite and facilitates strong interactions between the active electrode surface and analyte ions. On the other hand, GCGMMTCeCE can detect both  $\text{Fe}^{2+}/\text{Fe}^{3+}$  and  $\text{Ce}^{3+}/\text{Ce}^{4+}$  redox couples, with greater peak currents for sensitivity determination, but it exhibits different sensitivity variations for each analyte. Nonetheless, the quaternary composite matrix also promotes the formation of strong interactions between GCGMMTCeCE active electrode surface and analyte ions, resulting in higher sensitivities.

The limit of detection (LOD) is an important factor, defined as the lowest concentration of analyte that the electrode can measure. GMMTCeCE and GCGMMTCeCE have distinct values of LOD towards different analytes (refer to Table 3), with GMMTCeCE having a lower LOD for each analyte ion over GCGMMTCeCE. However, the results of both electrodes indicate that they can successfully detect  $\text{Fe}^{2+}$ ,  $\text{Fe}^{3+}$ ,  $\text{Ce}^{3+}$ , and  $\text{Ce}^{4+}$  ions in lower concentration levels. This is the remarkable achievement of graphite-clay composite electrode technology, which can be used in the development of sensor fabricating applications. Hence, these results confirm that GMMTCeCE and GCGMMTCeCE are well-suited for the detection of  $\text{Fe}^{2+}/\text{Fe}^{3+}$  and  $\text{Ce}^{3+}/\text{Ce}^{4+}$ , proving their ability to detect various inorganic ions and enhance the sensitivity through various modifications. Furthermore, GMMTCeCE accounts important candidate compared to GCGMMTCeCE due to its' better performance of detecting each ion and showing prominent sensitivity. The modification of electrode composite by different types of materials in these electrodes shows better enhancement in performance because these additional materials improve the characteristic features of the electroactive surfaces of these electrodes.

### 3.3 Electropolymerization using GMMTCeCE and GCGMMTCeCE

The electrodes, GMMTCeCE and GCGMMTCeCE are capable of detecting aniline as an organic material, they can be utilized to produce polyaniline (PANI) through electropolymerization. PANI is an organic conducting polymer that possesses remarkable characteristic features, including the existence of various oxidation states, environmental stability, redox reversibility, excellent conductivity, and processability [20]. Both electrodes obtained PANI successfully via the electropolymerization process, as confirmed by descriptive CVs with well-separated three peaks, demonstrating their ability to detect organic analytes as well as inorganic analytes (Figure 5a and 5b). Each electrode exhibits slightly different peak potentials and peak currents (Table 5), but the shape of CVs is quite similar to graphite-clay composite electrodes [1, 2, 4, 5, 9]. The prominent three peaks observed in the voltammograms account for three different oxidation states. Peak 1 is related to the half-oxidation of polyaniline denoted as the emeraldine form, peak 2 represents the fully oxidized state, pernigraniline form, while peak 3 depicts leucoemeraldine form the fully-reduced state, observed in both voltammograms [21]. When comparing each of these CVs, PANI-GCGMMTCeCE exhibits dominant peaks with relatively higher peak currents compared to PANI-GMMTCeCE, and the peak potentials are relatively lower than GMMTCeCE. However, both electrodes can produce better PANI coatings on active electrode surfaces, indicating their affinity for organic analytes, aided by the synergistic effect of the composites' matrix.

**Table 5.** Average peak potentials and peak currents related to Aniline electropolymerization of GMMTCeCE and GCGMMTCeCE

Electrode	Parameter	Peak 1	Peak 2	Peak 3
GMMTCeCE	$E$ (V)	0.379	0.807	0.552
	$I \times 10^{-3}$ (A)	0.959	1.303	0.745
GCGMMTCeCE	$E$ (V)	0.317	0.747	0.402
	$I \times 10^{-3}$ (A)	2.892	2.678	2.947

$E$ -average peak potential,  $I$ -average peak current

Electrochemical impedance spectroscopy (EIS) is a powerful technique used to investigate the electrochemical properties between polymer and electrode, as well as polymer and electrolyte [2, 3, 5]. Two slightly different Nyquist plots were obtained for PANI-GMMTCeCE and PANI-GCGMMTCeCE, which revealed closely to similar electrochemical properties of PANI obtained by each electrode (see Figure 6). Each spectrum has an equivalent circuit model confirmed by the literature (Figure 6) [22-24]. The EIS spectrum of PANI-GMMTCeCE consists of starting from a vertical straight line at the negative imaginary part, followed by the combined semi-arcs at the high-frequency region, and a tail at the low-frequency region. On the other hand, the EIS spectrum of PANI-GCGMMTCeCE has well-

separated semicircles at the high-frequency region, ending with an oblique followed by a tail at the low-frequency region. The values corresponding to each element included in the equivalent circuits tabulated in Table 6 separately for each electrode. In PANI-GMMTCeCE, the inductor ( $L$ ) generates the inductive effect by external artifacts like external wirings and the measurement system of PANI-GMMTCeCE [24]. This value of  $L$  indicates low inductance of the system at the ultra-high frequency region according to the values interpreted by the previous literature [25]. In contrast, there is no inductive effect at the beginning of the spectrum in PANI-GCGMTCeCE, confirming that the external circuit and wiring are fitted well without any winding formation.

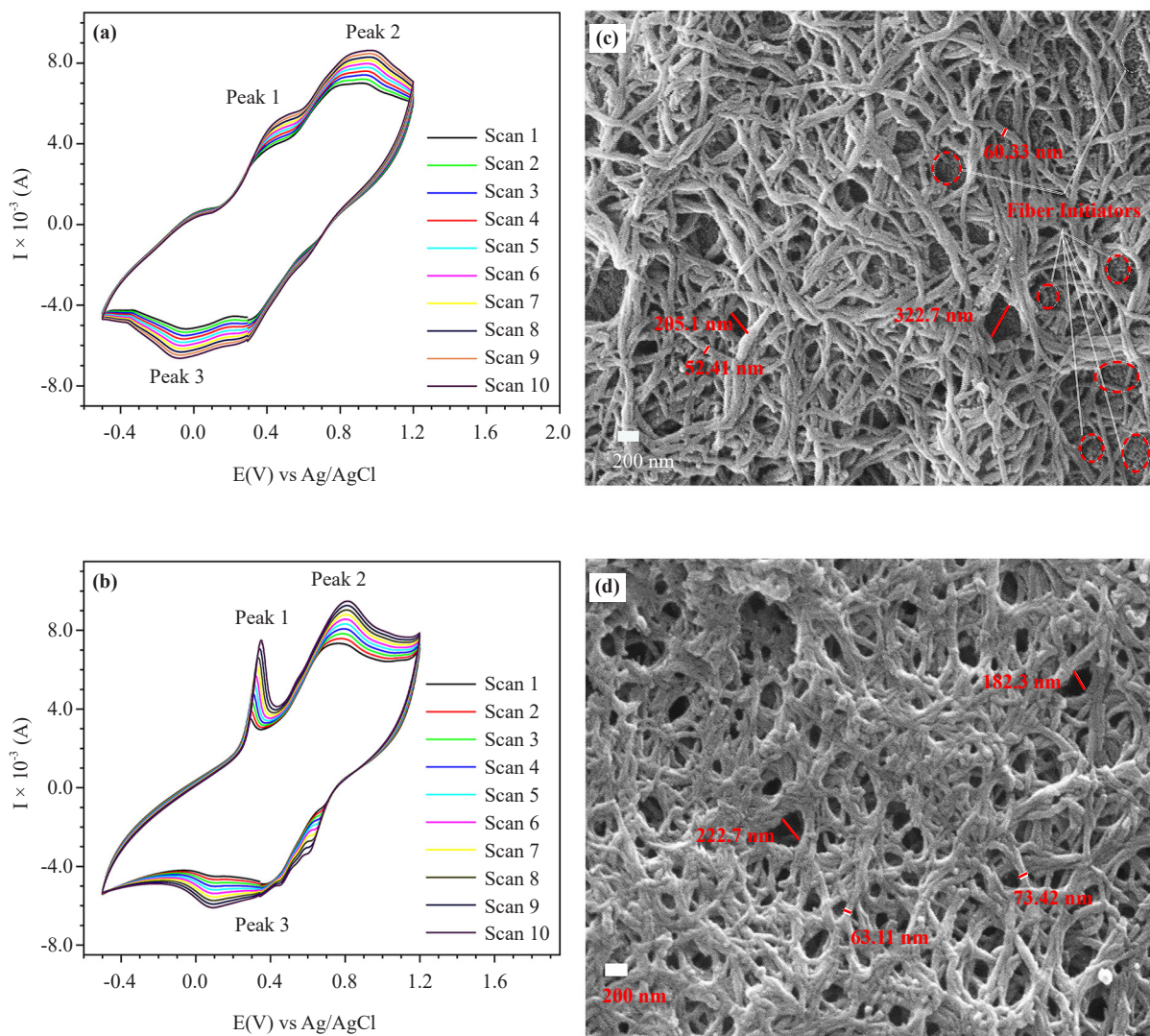


**Figure 5.** Cyclic Voltammograms obtained via electropolymerization of PANI onto; (a) GMMTCeCE; (b) GCGMTCeCE; SEM micrographs of PANI synthesized by electro-polymerization on each electrode's surface observed under the magnification ( $\times 50,000$ ); (c) PANI-GMMTCeCE (well-distributed PANI nanofibers network with multilayers, including polymer initiators); (d) PANI-GCGMTCeCE (densely packed PANI nanofibers network)

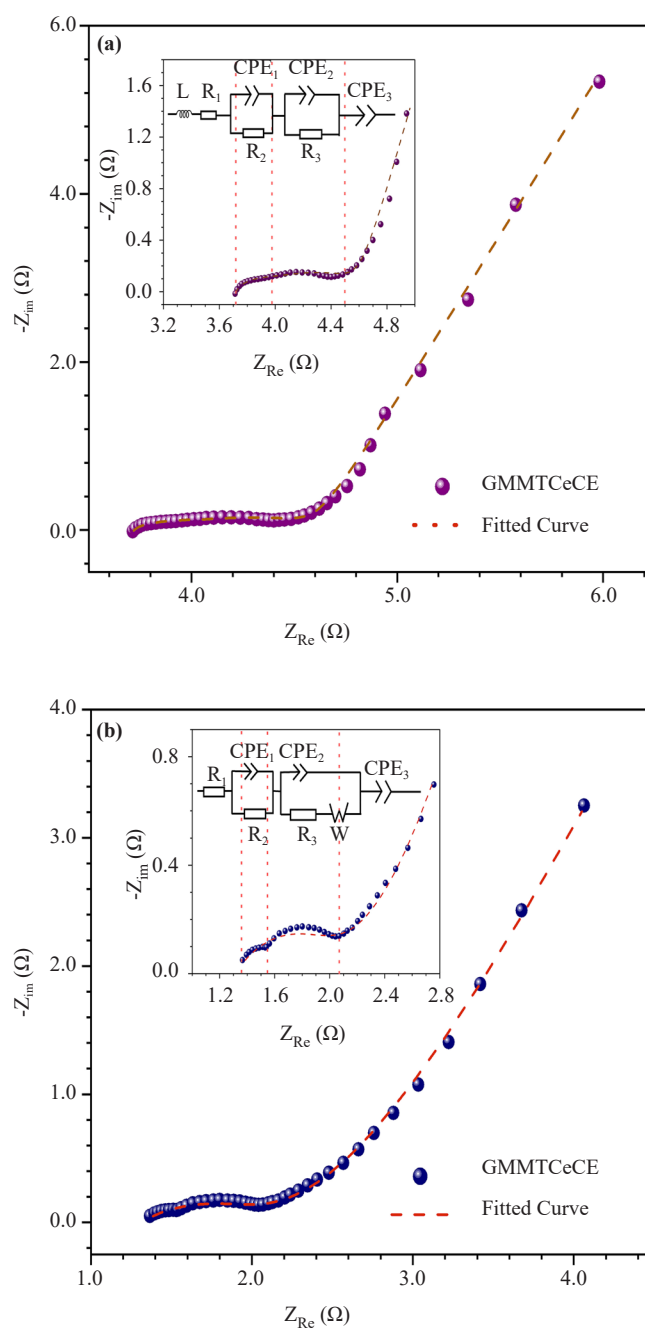


**Figure 6.** Nyquist plots related to PANI coated electrodes (insets of each Nyquist plot display at the high-frequency and the mid-frequency region with equivalent circuit model associated with each segment); (a) GMMTCeCE; (b) GCGMMTCeCE

Ohmic resistance ( $R_1$ ) is the total contributions of the PANI-coated electrode system's contact resistance and ohmic resistance, and it represents the intersection in the X-axis or starting point of the semicircular curve of the EIS spectrum [26]. It consists of the resistance of the electrolyte (1 M HCl), the intrinsic resistance of the composite materials of the electrode, and the contact resistance between the electroactive material (PANI) and current collector (Cu wire) [15, 22]. Comparing these two electrode systems, PANI-GCGMMTCeCE has a lower  $R_1$  than PANI-GMMTCeCE, but both  $R_1$  values are lower like PANI-GCGKCeCE, which was recently fabricated by authors, indicating better electrochemical performance in both systems [9]. Serial resistance, represented by  $R_2$ , indicates the strength of the PANI coating of the

electroactive surface in the electrode, accounting for the diameter of the first semicircle. Lower  $R_2$  corresponds to strong  $\pi$  interactions between PANI nuclei and graphite sheets in the electrode, while weaker  $\pi$  interactions cause higher  $R_2$  [2]. Both PANI-GMMTCeCE and PANI-GCGMMTCeCE show the lowest  $R_2$  values compared to PANI-coated previously fabricated graphite-clay composite electrodes, except PANI-GCGKCeCE as reported by authors [2-5, 9]. Among them, PANI-GCGKCeCE showcased the lowest  $R_2$  due to their remarkable villi-like PANI network, but these  $R_2$  values are also relatively closer than others [9]. Because of the modification of additional materials into the composite matrix, very stable and strong interactions could be formed between PANI nuclei and the electroactive surface of these electrodes. However, PANI-GMMTCeCE has the lowest  $R_2$ , suggesting ternary composite matrix enhances surface properties to strengthen these interfacial interactions rather than the quaternary composite matrix of PANI-GCGMMTCeCE. This reveals PANI coating of GMMTCeCE is strongly held together compared to GCGMMTCeCE's PANI coating.

**Table 6.** The fitted values of equivalent circuit elements related to Nyquist plots of PANI-GMMTCeCE and PANI-GCGMMTCeCE

Equivalent Circuit Element	Fitting Value	
	PANI-GMMTCeCE	PANI-GCGMMTCeCE
$L$	$8.29 \times 10^{-8}$ H	-
$R_1$	3.66 $\Omega$	1.31 $\Omega$
$R_2$	0.38 $\Omega$	0.64 $\Omega$
$R_3$	0.59 $\Omega$	1.47 $\Omega$
$Z_{CPE1}$	0.02 F s <sup>(<math>\alpha-1</math>)</sup>	0.04 F s <sup>(<math>\alpha-1</math>)</sup>
$Z_{CPE2}$	0.15 F s <sup>(<math>\alpha-1</math>)</sup>	1.51 F s <sup>(<math>\alpha-1</math>)</sup>
$Z_{CPE3}$	1.89 F s <sup>(<math>\alpha-1</math>)</sup>	3.23 F s <sup>(<math>\alpha-1</math>)</sup>
$n_1$	0.49	0.43
$n_2$	0.50	0.25
$n_3$	0.84	0.80
$Z_W$	-	304.70 $\Omega$ s <sup>-1/2</sup>

$L$ -Inductor,  $R_1$ ,  $R_2$ , and  $R_3$ -Resistors,  $Z_{CPE1}$ ,  $Z_{CPE2}$ , and  $Z_{CPE3}$ -Impedance corresponding to each constant phase element,  $n_1$ ,  $n_2$ ,  $n_3$ -numerical values related with each constant phase element,  $Z_W$ -Warburg element impedance

The diameter of the second semi-arc associated with charge transfer resistance, defined as  $R_3$ , represents the electrochemical kinetics behavior of the PANI-coated electrode system. Electrochemical kinetics depends on the factors attributed to PANI and electrodes' composite, including bandgap structure, particle integrity, particle size, and surface coating, which are used to interpret electrochemical reaction mechanisms [22]. In addition,  $R_3$  is inversely proportional to the heterogeneous electron transfer rate, which also can be used to describe the electrochemical kinetics of the system [14]. Similar to  $R_2$ ,  $R_3$  of both electrodes is lower than previously fabricated graphite-clay composite electrodes' PANI coating systems, excluding PANI-GCGKCeCE [9]. These results suggest that PANI coatings support higher electron transfer rates through remarkable improvements in the electroactive surface area of PANI-GMMTCeCE and PANI-GCGMMTCeCE. Moreover,  $R_3$  of PANI-GMMTCeCE is about three-fold lower than PANI-GCGMMTCeCE, revealing that PANI-GMMTCeCE system provides a significant surface area enhancement of PANI coating on the electroactive

surface in electrode rather than PANI-GCGMMTCeCE. The lower values of  $R_3$  indicate that PANI structures synthesized by these electrodes have a higher electroactive surface area, as confirmed by the PANI micrographs observed by SEM (Figure 5c and 5d). Both PANI structures consisted of PANI nanofibers, which provide high electroactive surface areas, resulting in higher conductivity of PANI compared to other PANI morphologies such as nanorods and nanospheres [27]. In terms of the size of PANI nanofibers, PANI-GMMTCeCE has relatively fine, well-distributed nanofibers rather than densely packed, relatively thicker PANI-GCGMMTCeCE nanofibers. Nanofibers in PANI-GMMTCeCE demonstrated their greater conductivity, achieved with lower  $R_3$  compared to PANI-GCGMMTCeCE nanofibers. Additionally, PANI-GMMTCeCE displays PANI monolayers, which contribute to initiating the polymerization and forming multi-layers of nanofibers. This is a remarkable feature of PANI observed for the first time among PANI coatings of graphite-clay composite electrodes. However, these features are absent in PANI-GCGMMTCeCE, indicating that PANI morphology depends on the electrode surface structure. Moreover, fiber density and distribution of PANI nanofibers, PANI-GMMTCeCE showcases well-distributed, thinner nanofibers with wider nanopores, resulting in a highly conductive polymer system. On the other hand, PANI-GCGMMTCeCE has densely packed, thick nanofibers with relatively narrow nanopores, limiting the generation of a conductive polymer system on the electrode surface. Based on the resulting values of  $R_1$ ,  $R_2$ , and  $R_3$ , the modification of the graphite-clay composite matrix by additional phases reinforces the electrochemical properties of the graphite-clay composite electrode and in addition, GMMTCeCE ternary composite electrode shows remarkable electrochemical properties than GCGMMTCeCE quaternary composite electrode.

In addition to resistances found in these circuits, three constant phase elements (CPE) appeared parallel to each of the resistances in both circuits that is a capacitive element consisting of double-layer capacitance and pseudocapitance. This element can be generated by association with factors in these PANI-coated electrode systems. They are the distribution of relaxation time caused by the non-uniform behavior in PANI-coated graphite composite electrode and HCl (electrolyte) interface, the porosity of PANI-coated electrode system, the nature of the materials in the electrode, and the dynamic disorder that occurred during the diffusion of electrolyte ions ( $H^+$  and  $Cl^-$ ) into PANI electrode system [27]. CPE describes the following equation 7 [26, 28].

$$Z_{CPE} = \frac{1}{Q(j\omega)^n} \quad (7)$$

Where  $Z_{CPE}$  is the impedance of CPE,  $Q$  is the frequency-independent constant depends on the PANI surface and electroactive substance (PANI), and  $\omega$  is the angular frequency ( $\omega = 2\pi f$ ) [28].  $n$  is the numerical variable between 0 and 1, related to the non-uniform distribution of current due to surface roughness and porosity of the PANI-coated electrode system [28].  $n = 0$  is defined as pure resistance,  $n = 1$  is the ideal capacitive behavior, and  $n > 0.5$  is the moderately capacitive behavior, those values are attributed to the characteristics of the PANI electrode system [28]. The presence of CPEs in the equivalent circuits describes the non-ideal capacitors of the system [22]. When comparing each of the impedance values of three CPEs of both PANI-coated electrode systems, these kinds of variations can be observed;  $Z_{CPE1} < Z_{CPE2} < Z_{CPE3}$  and  $Z_{CPE}(\text{PANI-GMMTCeCE}) < Z_{CPE}(\text{PANI-GCGMMTCeCE})$ . Therefore, the combination of pseudocapacitor and double-layer capacitor nature is comparatively greater in PANI-GCGMMTCeCE than in PANI-GMMTCeCE. Based on the values of  $n$  corresponding to each CPE, all  $n$  values of PANI-GMMTCeCE show moderate capacitive behavior, while only  $n_3$  of PANI-GCGMMTCeCE acts as a moderate capacitor. Despite the values of CPEs,  $n$  values of both electrodes follow the behavior as like this;  $n_1 < n_2 < n_3$  and  $n(\text{PANI-GMMTCeCE}) > n(\text{PANI-GCGMMTCeCE})$ . However, the presence of CPEs in both systems indicates that they are capable of demonstrating capacitive behavior, which suggests improved performance by modifying the composite matrix with additional phases of materials. Specifically, only the PANI-GCGMMTCeCE spectrum shows the Warburg element in the low-frequency region, which is linked to the limited diffusion process of ions from the electrolyte into the electroactive PANI coating [24, 29]. The impedance of the Warburg element can be expressed using equation 8 [15].

$$Z_W = \frac{\sigma}{\sqrt{\omega}} - j \frac{\sigma}{\sqrt{\omega}} \quad (8)$$

Where  $Z_w$ ,  $\sigma$ ,  $\omega$ , and  $j$  represent Warburg impedance, Warburg coefficient, angular frequency ( $\omega = 2\pi f$ ), and the imaginary number respectively. In conclusion, PANI-GMMTCeCE creates the best polymer-electrode system, which leads to remarkable electrochemical properties through synergetic interactions of ternary composite matrix and well-distributed PANI nanofibers network with multilayers of polymer. Also, PANI-GCGMMTCeCE produces an important system with good electrochemical features, aided by the synergetic effect created by the quaternary composite matrix and PANI nanofibers network. Furthermore, these EIS spectra suggest that the electrochemical characteristics of these PANI-coated electrode systems are closely related to battery and fuel cell applications rather than supercapacitor-like energy-storage devices.

### 3.4 Energy-storage devices (supercapacitors) of GMMTCeCE and GCGMMTCeCE

PANI-coated electrodes are well-suited for fabricating supercapacitor-like energy-storage devices due to their high charge density, good thermal stability, and low material cost [30]. Different types of PANI morphological structures, based on their size ranging from micro-meter-sized to nanofibers, were observed by the previously fabricated graphite-clay composite electrodes and other related literature on PANI [2-5, 9, 14, 31-33]. PANI nanostructures, which are the most prominent morphological types, exhibited as nanorods, nanospheres, and nanofibers, have the potential to perform as conductive layers in different applications [34]. PANI-GMMTCeCE and PANI-GCGMMTCeCE show nano-meter-sized fiber networks that are capable of fabricating supercapacitor devices since their higher electroactive surface area can efficiently store charge (see Figure 6a and 6b). Both of these electrodes coated with PANI, were utilized to construct the supercapacitor cells with evaluating the performance of each of them. Both supercapacitor cells were constructed using electropolymerized PANI by 100 cycles of CV, which is deemed as the optimum number of cyclic voltammogram cycles based on the previous results of graphite-clay composite electrodes developed by authors [4, 9].

Cyclic voltammograms of both supercapacitor cells at different scan rates provide a comparative estimation of each cell's specific capacitance ( $C_s$ ) (Figure 7a and 7b). These CVs offer some insights into the capacitive properties, such as pseudocapacitance by showcasing peaks related to the redox chemical reactions in PANI-coated electrode systems. The peaks are more prominent at lower scan rates, when increasing scan rates sequentially they diminished. These peaks indicate the pseudocapacitance behavior of the PANI-coated electrode system, which is further confirmed by the presence of CPEs in both EIS spectra.  $C_s$  decreases as the scan rate increases in CVs, and the highest  $C_s$  was observed in both supercapacitor cells at the lowest scan rate ( $5 \text{ mV}\cdot\text{s}^{-1}$ ). Since the scan rate plays a significant role in electrode transfer and ion diffusion of the electrolyte, lower scan rates are supposed to facilitate efficient electrode ion diffusion between PANI-electrolyte's external interface and PANI's active pore sites [15]. In contrast, electrolyte ion diffusion is limited by slowing down the doping/dedoping process of PANI at higher scan rates, resulting in the reduction of  $C_s$  [15]. The reduction of  $C_s$  is observed in a polynomial manner in the PANI-GMMTCeCE cell, while the PANI-GCGMMTCeCE cell shows a linear decrease of  $C_s$  when changing the scan rate from  $5 \text{ mV}\cdot\text{s}^{-1}$  to  $25 \text{ mV}\cdot\text{s}^{-1}$  (Figure 7c). However, both CVs depict the stability of both supercapacitor cells when changing the scan rates.

PANI nanofiber networks present in both electrodes indicate that both supercapacitors are capable of delivering higher  $C_s$  and functioning as better energy storage devices (Table 7). Even though the highest  $C_s$ , which is observed at  $5 \text{ mV}\cdot\text{s}^{-1}$  in both supercapacitor devices, the highest  $C_s$  accounts for the PANI-GMMTCeCE device. Multi-layer PANI network, composed of nano projections (polymer initiators) and a well-distributed nanofiber network in GMMTCeCE influences the attainment of higher  $C_s$ . This remarkable PANI morphological structure contributes to the formation of strong interactions between PANI and GMMTCeCE surface, which enhances the charge storage mechanism in supercapacitor cells. Graphite, MMT, and cement composite matrix can effectively enhance the surface features in electrodes, thereby producing PANI nanofibers with significant morphological characters. In contrast, PANI-GCGMMTCeCE generates lower  $C_s$  than PANI-GMMTCeCE due to the densely-packed nanofibers on PANI and the absence of a multi-layer network of PANI. PANI-GCGMMTCeCE exhibits a densely packed nanofiber network that is less effective for charge storage and produces moderately strong interactions of PANI and the electrode surface of GCGMMTCeCE. The addition of colloidal graphite into the composite matrix modifies the electrode surface to initiate electropolymerization and obtain a better coating, but the resulting effect is lower compared to GMMTCeCE. PANI-GMMTCeCE with its' nanofiber network accounts for higher  $C_s$ , closely similar to the value ( $1,029 \text{ F}\cdot\text{g}^{-1}$  at  $5 \text{ mV}\cdot\text{s}^{-1}$ ) of recently fabricated PANI-GCGKCeCE supercapacitor cell [9]. However, PANI-GCGMMTCeCE shows higher  $C_s$ , which is closer to  $C_s$  ( $782 \text{ F}\cdot\text{g}^{-1}$  at  $5 \text{ mV}\cdot\text{s}^{-1}$ ) in PANI-GCGMMTCeCE

supercapacitor device, while PANI-GMMTCE with  $C_s$  ( $342 \text{ F}\cdot\text{g}^{-1}$  at  $5 \text{ mV}\cdot\text{s}^{-1}$ ) is comparatively low manufactured previously by authors [3, 4]. All of these supercapacitor devices performed with higher  $C_s$ , generated by PANI nanofiber networks with strong interactions on graphite-clay composite electrode surfaces.  $C_s$  values of PANI-GMMTCeCE and PANI-GCGMMTCeCE are greater than the supercapacitor devices fabricated using different PANI morphologies, including PANI aerogels ( $184 \text{ F}\cdot\text{g}^{-1}$ ) [35], PANI nanofibers ( $252 \text{ F}\cdot\text{g}^{-1}$ ) [36], PANI nanorods ( $297 \text{ F}\cdot\text{g}^{-1}$ ) [37], PANI nanospheres ( $345 \text{ F}\cdot\text{g}^{-1}$ ) [34], nanoporous PANI ( $350 \text{ F}\cdot\text{g}^{-1}$ ) [38], PANI hydrogels ( $450 \text{ F}\cdot\text{g}^{-1}$ ) [39], PANI nanogranules ( $500 \text{ F}\cdot\text{g}^{-1}$ ) [40], PANI nanocapsules ( $502 \text{ F}\cdot\text{g}^{-1}$ ) [41]. Moreover, PANI nanotubes ( $714 \text{ F}\cdot\text{g}^{-1}$ ) [42, 43], PANI nanolayers ( $738 \text{ F}\cdot\text{g}^{-1}$ ) [44], PANI nanobelts ( $873 \text{ F}\cdot\text{g}^{-1}$ ) [45], and PANI nanowires ( $950 \text{ F}\cdot\text{g}^{-1}$ ) [46] mentioned in literature are shown lower  $C_s$  compared to PANI-GMMTCeCE, revealing its good performance related to charge storage. GMMTCeCE composite matrix effectively contributes to creating a well-suited electrode' surface, resulting in the production of an effective PANI nanofiber network, leading to obtaining a higher capacitive character. While the PANI nanofiber network generated by GCGMMTCeCE is less dominant over GMMTCeCE, it also contributes to producing substantial capacitive character in supercapacitor cells.

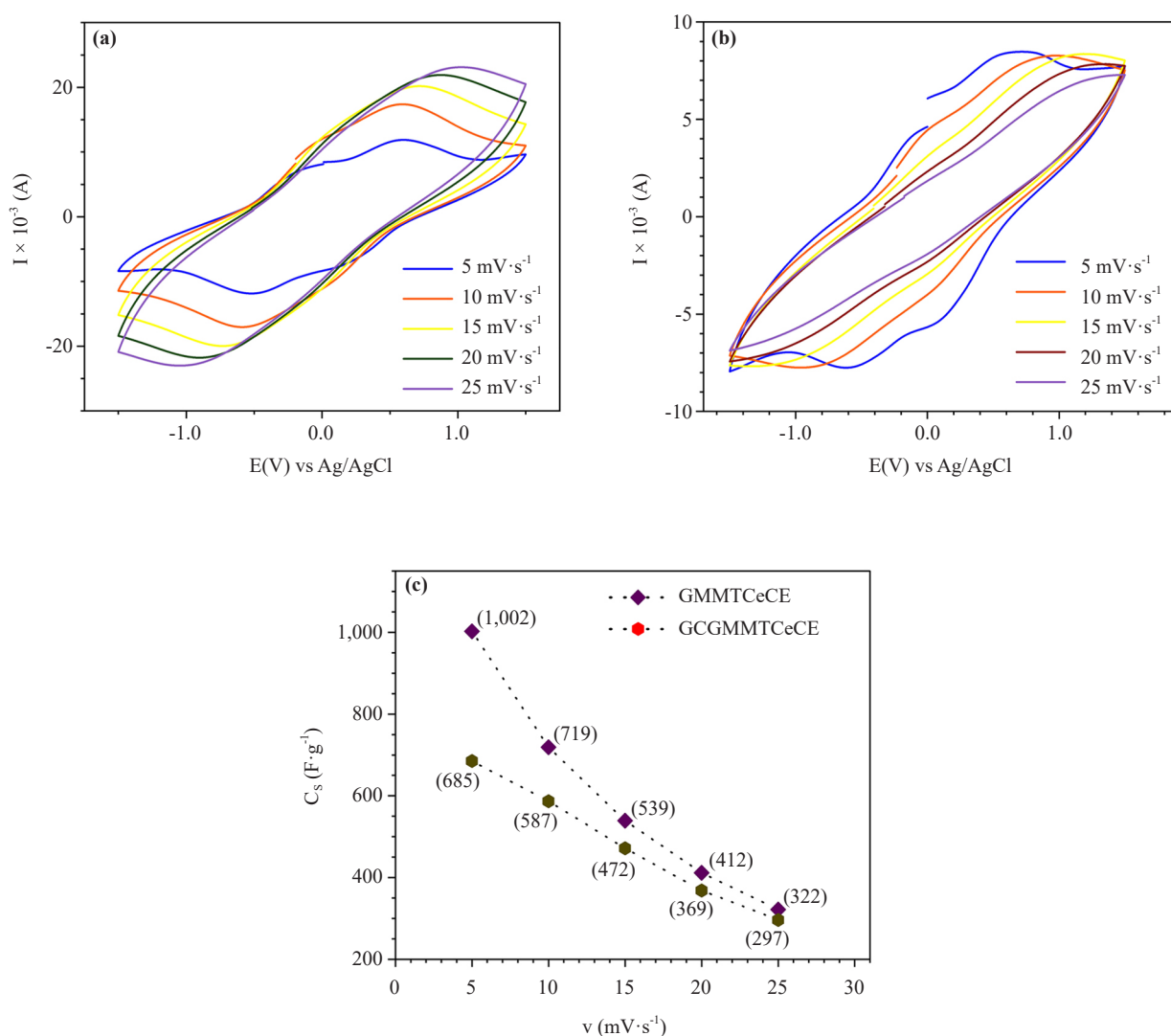


**Figure 7.** Specific capacitance at different scan rates of supercapacitor cells developed using PANI-coated electrodes; (a) CVs of GMMTCeCE; (b) CVs of GCGMMTCeCE; (c) Specific capacitance as a function of scan rate for GMMTCeCE and GCGMMTCeCE supercapacitor cells

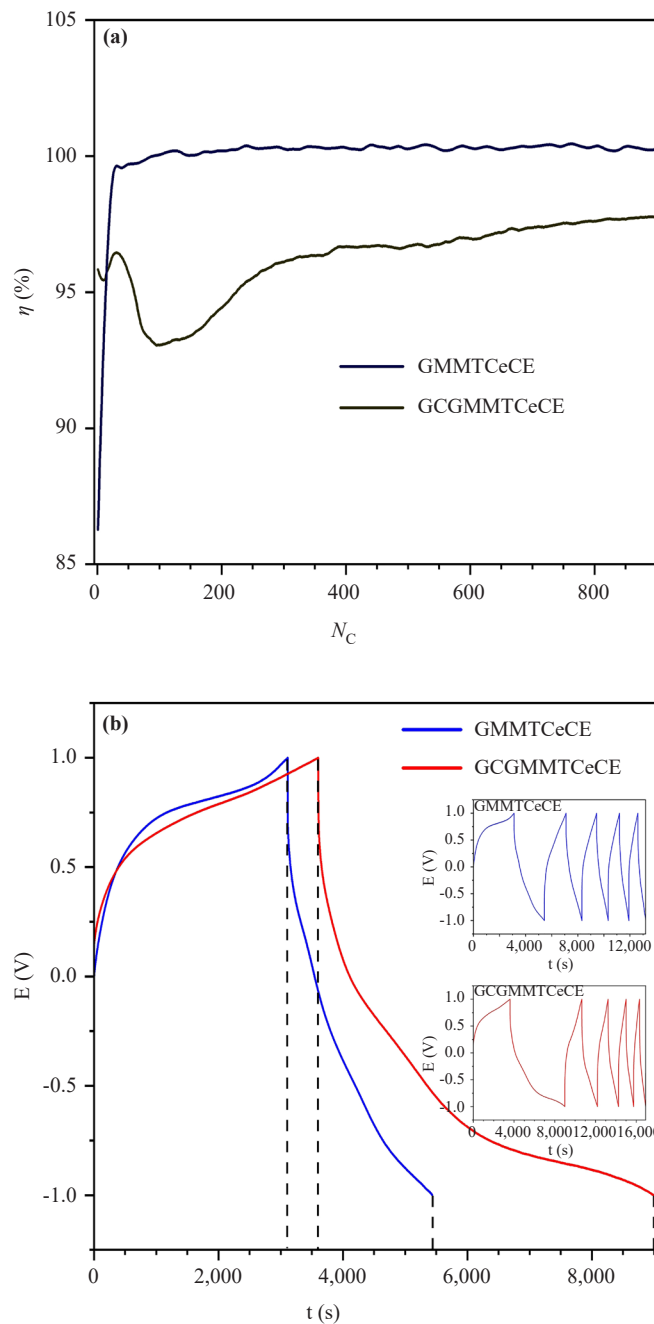


**Figure 8.** (a) Coulombic efficiency variation of fabricated supercapacitor cell using PANI-GMMTCeCE and PANI-GCGMMTCeCE up to 900 cycles [ $\eta$  and  $N_c$  denote the Coulombic efficiency (%) and number of charge discharge cycles respectively]; (b) 1<sup>st</sup> cycle of GCD in both supercapacitors (inset displays cyclic variation of galvanostatic charge discharge curves of; PANI-GMMTCeCE Supercapacitor cell and PANI-GCGMMTCeCE Supercapacitor cell)

The galvanostatic charge-discharge (GCD) technique was used to assess the cyclic stability of charge-discharge processes in supercapacitor cells. Both supercapacitor cells underwent 900 cycles of charge-discharge, and their performance was evaluated using Coulombic efficiency. Figure 8a shows the variation of Coulombic efficiency ( $\eta$ ) of both supercapacitor cells and both cells consistently maintained higher  $\eta$  value throughout their cycles. PANI-GMMTCeCE cell depicts a significant increment of  $\eta$  value at the beginning GCD process and then consistently maintained a value close to 100% with minimal fluctuations until the end. On the other hand, PANI-GCGMMTCeCE

cell exhibited significant fluctuation in  $\eta$  value at the start but then it stabilized at about 96% until the end. GCD curves of PANI-GMMTCeCE and PANI-GCGMMTCeCE supercapacitor cells (see Figure 8b) indicate identical charge-storing processes, which are associated with PANI-coated cell systems. The presence of a well-distributed, thinner nanofiber network in PANI-GMMTCeCE with nanometer-sized pores facilitates the successful establishment of ion migration paths for electrolyte ion penetration and enhances the activation of charge storage sites (nanopores) on PANI [9]. In contrast, PANI-GCGMMTCeCE exhibits relatively less amount of the process of creating ion migration paths and activation of charge storage sites due to the densely packed nanofiber network. As a result, PANI-GMMTCeCE ultimately enhances the charge-storing capacity of supercapacitor cells compared to PANI-GCGMMTCeCE. Higher  $\eta$  values indicate a higher charge-storing capacity, leading to improved cyclic stability and a longer life span of the supercapacitor cell [47]. PANI-GMMTCeCE and PANI-GCGMMTCeCE supercapacitor cells demonstrate higher  $\eta$  values, indicating better cyclic stability and longer life span. Considering the shape of GCD curves, both supercapacitor cells exhibit similar charge-discharge curves, suggesting identical behavior of charge-storage mechanisms. The combination of graphite, MMT, and cement in GMMTCeCE synergistically enhances the composite matrix, facilitating to attainment of a well-characterized PANI nanofiber network, resulting in highly performed supercapacitor achieving higher specific capacitance and better cyclic stability, demonstrating its potential of energy-storage applications. Similar to GMMTCeCE, GCGMMTCeCE matrix also contributes to the formation of PANI nanofiber network, allowing to fabrication of supercapacitors with good performance, including higher specific capacitance and good cyclic stability. These composite electrodes can be further developed to fabricate supercapacitor devices using different conductive polymers to achieve even better performance and higher energy storage capacity.

**Table 7.** Specific Capacitance of supercapacitor cell based on CV and GCD

Supercapacitor	Specific Capacitance/F·g <sup>-1</sup>	
	CV	GCD
PANI-GMMTCeCE	1,002	1,105
PANI-GCGMMTCeCE	685	769

## 4. Conclusions

Graphite-MMT-cement ternary composite electrode (GMMTCeCE) and graphite-colloidal graphite-MMT-cement quaternary composite electrode (GCGMMTCeCE) are fabricated modifying the composite matrices via mechanical and thermal treatment to improve the performance in electroanalytical and energy storage applications. The GMMTCeCE exhibits the lowest resistivity, which is  $1.59 \times 10^{-3} \Omega \cdot m$  compared to that of GCGMMTCeCE ( $3.65 \times 10^{-3} \Omega \cdot m$ ), while both electrodes account for an improved mechanical strength. The electrode strength and conductivity entirely depend on its microstructure as the highly compressed GMMTCeCE accounts for the uniformly packed graphite sheets, in contrast to GCGMMTCeCE which consists of cluster-like graphite sheets, resulting in the highest resistivity. The GMMTCeCE exhibits the narrow  $\Delta E_p$  and higher electrode sensitivity to all analytes in comparison with GCGMMTCeCE. In contrast, GCGMMTCeCE accounts for polynomial sensitivity distribution for some analytes, including PHCFT and CST, suggesting that interactions between the analyte and GCGMMTCeCE surface are rather complex. The multilayered PANI nanofiber network that is evenly distributed on GMMTCeCE accounts for the lowest serial (0.38  $\Omega$ ) and charge transfer (0.59  $\Omega$ ) resistance in comparison with GCGMMTCeCE, which is attributed to 0.64  $\Omega$  serial and 1.47  $\Omega$  charge transfer resistance, respectively. The specific capacitance measured using a device, which is fabricated with identical PANI coated electrodes exhibits high values, including 1,002 F·g<sup>-1</sup> at 5 mV·s<sup>-1</sup> and 685 F·g<sup>-1</sup> at 5 mV·s<sup>-1</sup> for GMMTCeCE and GCGMMTCeCE, respectively. The supercapacitor cells that are fabricated with both electrode types attributed to a better cyclic stability that indicates improved long-term usability. In summary, GMMTCeCE and GCGMMTCeCE are fabricated with low-cost raw materials to leverage synergistic effects in

composite matrices in electroanalytical and energy-storage applications. GMMTCeCE outperformed GCGMMTCeCE in analyte detection, electro-polymerization, and supercapacitor performance. These electrodes hold better potency for further developments in fabricating sensors and highly efficient supercapacitor devices.

## Acknowledgement

This work was financially supported by the Industrial Technology Institute of Sri Lanka (Grant No. TG 24/246).

## Conflict of interest

The authors have no competing interests to declare that are relevant to the content of this article.

## References

- [1] Karunadasa KSP, Manoratne CH, Pitawala HMTGA, Rajapakse RMG. A potential working electrode based on graphite and montmorillonite for electrochemical applications in both aqueous and molten salt electrolytes. *Electrochemistry Communications*. 2019; 108: 106562.
- [2] Karunadasa KSP, Rathnayake D, Manoratne C, Pitawala A, Rajapakse G. A binder-free composite of graphite and kaolinite as a stable working electrode for general electrochemical applications. *Electrochemical Science Advances*. 2021; 1(4): e2100003.
- [3] Rathnayake DT, Karunadasa KSP, Wijekoon ASK, Manoratne CH, Gamini Rajapakse RM, Pitawala HMTGA. Polyaniline-conjugated graphite-montmorillonite composite electrode prepared by in situ electropolymerization for supercapacitor applications. *Chemical Papers*. 2023; 77(5): 2923-2928.
- [4] Madhushanka PMH, Karunadasa KSP, Gamini Rajapakse RM, Manoratne CH, Bandara HMN. Low-cost composite electrode consisting of graphite, colloidal graphite and montmorillonite with enhanced electrochemical performance for general electroanalytical techniques and device fabrication. *Chemical Papers*. 2024; 78(1): 633-643.
- [5] Rathnayake DT, Karunadasa KSP, Wijekoon ASK, Manoratne CH, Rajapakse RMG. Low-cost ternary composite of graphite, kaolinite and cement as a potential working electrode for general electrochemical applications. *Chemical Papers*. 2022; 76(10): 6653-6658.
- [6] Bellido-Milla D, Cubillana-Aguilera LM, El Kaoutit M, Hernández-Artiga MP, Hidalgo-Hidalgo de Cisneros JL, Naranjo-Rodríguez I, et al. Recent advances in graphite powder-based electrodes. *Analytical and Bioanalytical Chemistry*. 2013; 405(11): 3525-3539.
- [7] Wring SA, Hart JP. Chemically modified, carbon-based electrodes and their application as electrochemical sensors for the analysis of biologically important compounds. A review. *Analyst*. 1992; 117(8): 1215-1229. Available from: <https://doi.org/10.1039/AN9921701215>.
- [8] Smith MA. A Consideration of graphite electrodes. *IEEE Transactions on Industry Applications*. 1982; IA-18(4): 431-434.
- [9] Madhushanka PMH, Karunadasa KSP, Rajapakse RMG. Graphite-colloidal graphite-kaolinite-cement quaternary composite electrode with improved synergetic matrix effect towards efficient energy storage and electroanalytical applications. *Chemical Papers*. 2024; 78: 5585-5598. Available from: <https://doi.org/10.1007/s11696-024-03502-6>.
- [10] Okpoli CC. Sensitivity and resolution capacity of electrode configurations. *International Journal of Geophysics*. 2013; 2013: 608037.
- [11] Temenoff JS, Mikos AG. *Biomaterials: The intersection of biology and materials science*. Upper Saddle River: Pearson/Prentice Hall; 2008.
- [12] Kunz AH. The reduction potential of the ceric-cerous electrode. *Journal of the American Chemical Society*. 1931; 53(1): 98-102.
- [13] Smith GF, Getz CA. Cerate oxidimetry. *Industrial & Engineering Chemistry Analytical Edition*. 1938; 10(4): 191-195.
- [14] Mondal S, Sangaranarayanan MV. Permselectivity and thickness-dependent ion transport properties of overoxidized

- polyaniline: A mechanistic investigation. *Physical Chemistry Chemical Physics*. 2016; 18(44): 30705-30720. Available from: <https://doi.org/10.1039/C6CP04975C>.
- [15] Xie Y, Du H. Electrochemical capacitance of a carbon quantum dots-polypyrrole/titania nanotube hybrid. *Rsc Advances*. 2015; 5(109): 89689-89697.
- [16] Chanda M. Electrical, electronic and optical properties. In: *Science of Engineering Materials: Volume 3 Engineering Properties*. London: Macmillan Education UK; 1980. p.61-126. Available from: [https://doi.org/10.1007/978-1-349-06055-9\\_2](https://doi.org/10.1007/978-1-349-06055-9_2).
- [17] Elgrishi N, Rountree KJ, McCarthy BD, Rountree ES, Eisenhart TT, Dempsey JL. A practical beginner's guide to cyclic voltammetry. *Journal of Chemical Education*. 2018; 95(2): 197-206.
- [18] Ngamchuea K, Eloul S, Tschulik K, Compton RG. Planar diffusion to macro disc electrodes-what electrode size is required for the Cottrell and Randles-Sevcik equations to apply quantitatively? *Journal of Solid State Electrochemistry*. 2014; 18(12): 3251-3257.
- [19] Mirceski V, Gulaboski R, Lovric M, Bogeski I, Kappl R, Hoth M. Square-wave voltammetry: A review on the recent progress. *Electroanalysis*. 2013; 25(11): 2411-2422.
- [20] Syed AA, Dinesan MK. Review: Polyaniline-A novel polymeric material. *Talanta*. 1991; 38(8): 815-837.
- [21] Song E, Choi J-W. Conducting polyaniline nanowire and its applications in chemiresistive sensing. *Nanomaterials*. 2013; 3(3): 498-523.
- [22] Chen B-R, Police YR, Li M, Chinnam PR, Tanim TR, Dufek EJ. A mathematical approach to survey electrochemical impedance spectroscopy for aging in lithium-ion batteries. *Frontiers in Energy Research*. 2023; 11: 167.
- [23] Shanthi PM, Hanumantha PJ, Ramalinga K, Gattu B, Datta MK, Kumta PN. Sulfonic acid based complex framework materials (cfm): Nanostructured polysulfide immobilization systems for rechargeable lithium-sulfur battery. *Journal of The Electrochemical Society*. 2019; 166(10): A1827.
- [24] Zhang Ja, Wang P, Liu Y, Cheng Z. Variable-order equivalent circuit modeling and state of charge estimation of lithium-ion battery based on electrochemical impedance spectroscopy. *Energies*. 2021; 14(3): 769.
- [25] Cruz-Manzo S. Further understanding of uncertainties in the impedance spectrum of the polymer electrolyte fuel cell due to inductive effects and oxygen diffusion time constant. *Journal of Energy and Power Technology*. 2020; 2(4): 17.
- [26] Dhirde AM, Dale NV, Salehfar H, Mann MD, Han TH. Equivalent electric circuit modeling and performance analysis of a PEM fuel cell stack using impedance spectroscopy. *IEEE Transactions on Energy Conversion*. 2010; 25(3): 778-786.
- [27] Dubal DP, Lee SH, Kim JG, Kim WB, Lokhande CD. Porous polypyrrole clusters prepared by electropolymerization for a high performance supercapacitor. *Journal of Materials Chemistry*. 2012; 22(7): 3044-3052. Available from: <https://doi.org/10.1039/C2JM14470K>.
- [28] Du H, Xie Y, Xia C, Wang W, Tian F. Electrochemical capacitance of polypyrrole-titanium nitride and polypyrrole-titania nanotube hybrids. *New Journal of Chemistry*. 2014; 38(3): 1284-1293. Available from: <https://doi.org/10.1039/C3NJ01286G>.
- [29] Oldenburger M, Bedürftig B, Gruhle A, Grimsman F, Richter E, Findeisen R, et al. Investigation of the low frequency Warburg impedance of Li-ion cells by frequency domain measurements. *Journal of Energy Storage*. 2019; 21: 272-280.
- [30] Rudge A, Raistrick I, Gottesfeld S, Ferraris JP. A study of the electrochemical properties of conducting polymers for application in electrochemical capacitors. *Electrochimica Acta*. 1994; 39(2): 273-287.
- [31] Mehdinia A, Dejaloud M, Jabbari A. Nanostructured polyaniline-coated anode for improving microbial fuel cell power output. *Chemical Papers*. 2013; 67(8): 1096-1102.
- [32] Wang H, Lin J, Shen ZX. Polyaniline (PANi) based electrode materials for energy storage and conversion. *Journal of Science: Advanced Materials and Devices*. 2016; 1(3): 225-255.
- [33] Wang Q, Li JL, Gao F, Li WS, Wu KZ, Wang XD. Activated carbon coated with polyaniline as an electrode material in supercapacitors. *New Carbon Materials*. 2008; 23(3): 275-280.
- [34] Chen W, Rakhi RB, Alshareef HN. Morphology-dependent enhancement of the pseudocapacitance of template-guided tunable polyaniline nanostructures. *The Journal of Physical Chemistry C*. 2013; 117(29): 15009-15019.
- [35] Zhao H-B, Yuan L, Fu Z-B, Wang C-Y, Yang X, Zhu J-Y, et al. Biomass-based mechanically strong and electrically conductive polymer aerogels and their application for supercapacitors. *ACS Applied Materials & Interfaces*. 2016; 8(15): 9917-9924.
- [36] Huang H, Zeng X, Li W, Wang H, Wang Q, Yang Y. Reinforced conducting hydrogels prepared from the in situ polymerization of aniline in an aqueous solution of sodium alginate. *Journal of Materials Chemistry A*. 2014;

2(39): 16516-16522. Available from: <https://doi.org/10.1039/C4TA03332A>.

- [37] Wang X, Deng J, Duan X, Liu D, Guo J, Liu P. Crosslinked polyaniline nanorods with improved electrochemical performance as electrode material for supercapacitors. *Journal of Materials Chemistry A*. 2014; 2(31): 12323-12329. Available from: <https://doi.org/10.1039/C4TA02231A>.
- [38] Gawli Y, Banerjee A, Dhakras D, Deo M, Bulani D, Wadgaonkar P, et al. 3D polyaniline architecture by concurrent inorganic and organic acid doping for superior and robust high rate supercapacitor performance. *Scientific Reports*. 2016; 6(1): 21002.
- [39] Pan L, Yu G, Zhai D, Lee HR, Zhao W, Liu N, et al. Hierarchical nanostructured conducting polymer hydrogel with high electrochemical activity. *Proceedings of the National Academy of Sciences*. 2012; 109(24): 9287-9292.
- [40] Li X, Li X, Dai N, Wang G, Wang Z. Preparation and electrochemical capacitance performances of superhydrophilic conducting polyaniline. *Journal of Power Sources*. 2010; 195(16): 5417-5421.
- [41] Yang W, Gao Z, Song N, Zhang Y, Yang Y, Wang J. Synthesis of hollow polyaniline nano-capsules and their supercapacitor application. *Journal of Power Sources*. 2014; 272: 915-921.
- [42] Sk MM, Yue CY. Synthesis of polyaniline nanotubes using the self-assembly behavior of vitamin C: A mechanistic study and application in electrochemical supercapacitors. *Journal of Materials Chemistry A*. 2014; 2(8): 2830-2838. Available from: <https://doi.org/10.1039/C3TA14309K>.
- [43] Karunadasa K, Manoratne C. Pitawala HMTGA, Rajapakse RMG. Thermal decomposition of calcium carbonate (calcite polymorph) as examined by in-situ high-temperature X-ray powder diffraction. *Journal of Physics and Chemistry of Solids*. 2019; 134: 21-28.
- [44] Sumboja A, Wang X, Yan J, Lee PS. Nanoarchitected current collector for high rate capability of polyaniline based supercapacitor electrode. *Electrochimica Acta*. 2012; 65: 190-195.
- [45] Li G-R, Feng Z-P, Zhong J-H, Wang Z-L, Tong Y-X. Electrochemical synthesis of polyaniline nanobelts with predominant electrochemical performances. *Macromolecules*. 2010; 43(5): 2178-2183.
- [46] Wang K, Huang J, Wei Z. Conducting polyaniline nanowire arrays for high performance supercapacitors. *The Journal of Physical Chemistry C*. 2010; 114(17): 8062-8067.
- [47] Sarkar S, Akshaya R, Ghosh S. Nitrogen doped graphene/CuCr<sub>2</sub>O<sub>4</sub> nanocomposites for supercapacitors application: Effect of nitrogen doping on coulombic efficiency. *Electrochimica Acta*. 2020; 332: 135368. Available from: <https://doi.org/10.1016/j.electacta.2019.135368>.

## Appendix A

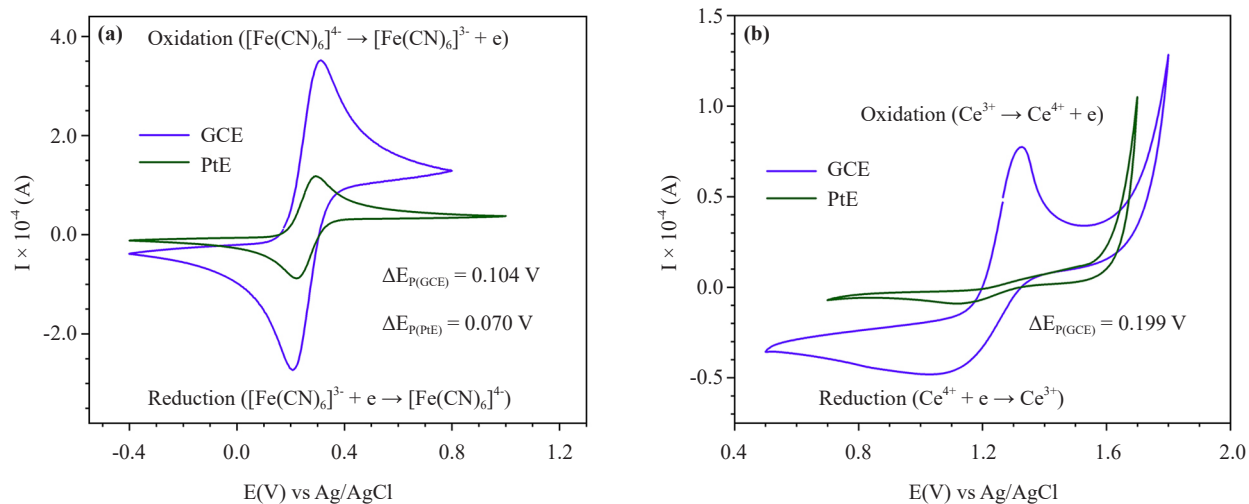


**Figure A1.** CV curves related to analyte detection using GCE and PtE; (a)  $\text{Fe}^{2+}/\text{Fe}^{3+}$  detection by PHCFT analyte; (b)  $\text{Ce}^{3+}/\text{Ce}^{4+}$  detection by CST analyte [ $\Delta E_p$  denotes peak-to-peak separation]

## Appendix B

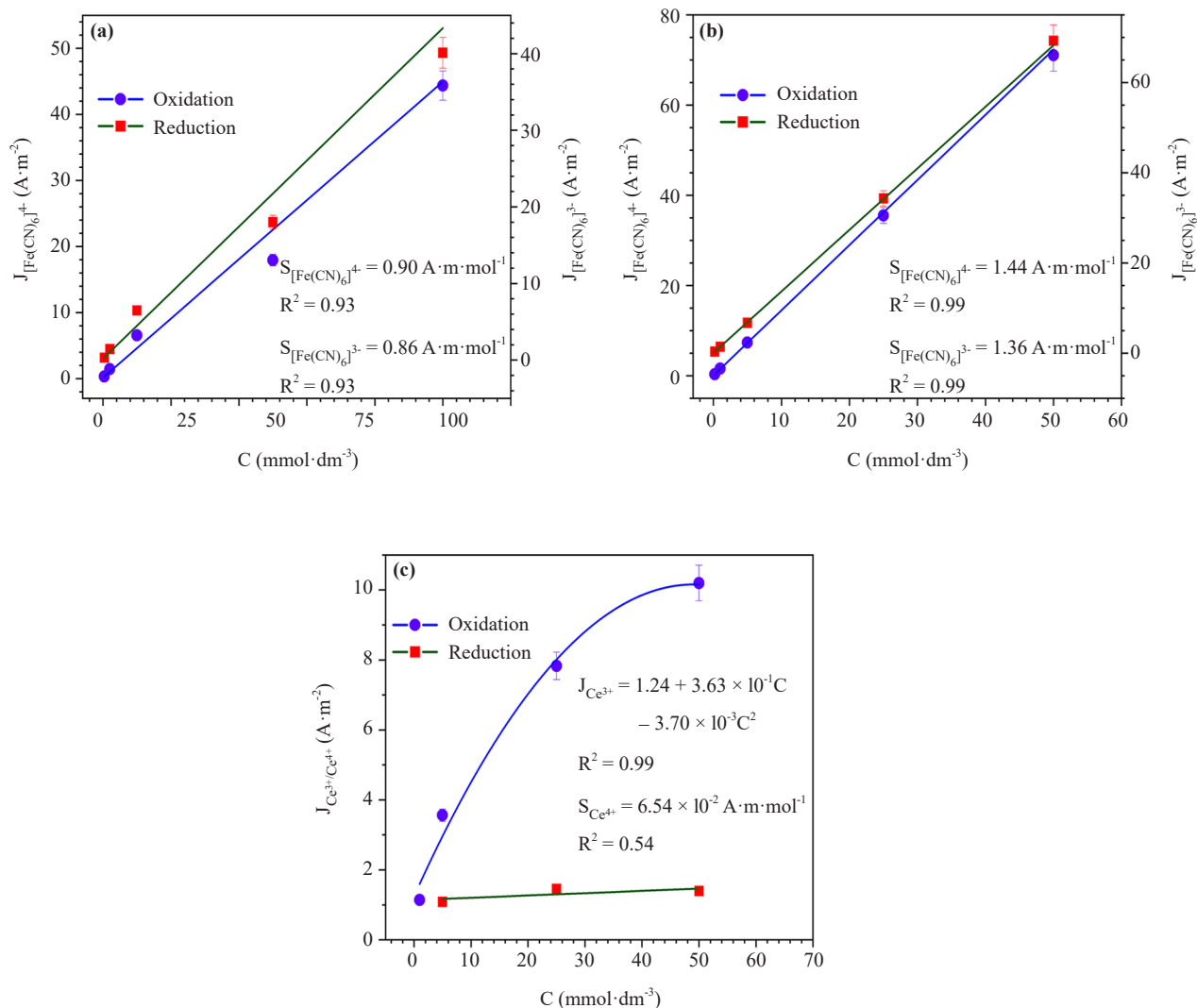


**Figure B1.** GCE and PtE sensitivities towards different analyte species; (a) Fe<sup>2+</sup>/Fe<sup>3+</sup> sensitivities of GCE by PHCFT; (b) Fe<sup>2+</sup>/Fe<sup>3+</sup> sensitivities of PtE by PHCFT; (c) Ce<sup>3+</sup>/Ce<sup>4+</sup> sensitivities of GCE by CST [J, C, and S denote the current density (A·m<sup>-2</sup>), analyte concentration (mmol·dm<sup>-3</sup>), and sensitivity of each analyte species (A·m·mol<sup>-1</sup>), respectively.]